January 2012

Investigation and Synthesis of Novel Graphene-Based Nanocomposites for Hydrogen Storage

Anthony Joseph D'angelo
University of South Florida, adangel2@mail.usf.edu

Investigation and Synthesis of Novel Graphene-Based Nanocomposites for Hydrogen Storage

by

Anthony Joseph D'Angelo

A thesis submitted in partial fulfillment
of the requirements for the degree of
Master of Science in Chemical Engineering
Department of Chemical and Biomedical Engineering
College of Engineering
University of South Florida

Co-Major Professor: D. Yogi Goswami, Ph.D.
Co-Major Professor: Elias Stefanakos, Ph.D.
Manoj Ram, Ph.D.
John Kuhn, Ph.D.

Date of Approval:
March 22, 2012

Keywords: cross-linking, physisorption, exfoliation, adsorption enthalpy, metal doping

Dedication

This thesis is dedicated to my parents, Margarita D'Angelo and George D'Angelo, and my step-father, Tony Cicarella, for it is they who gave me the opportunity to pursue higher education. Their financial and emotional support assisted me throughout my education.

I especially want to thank my mother. Her unconditional love and guidance throughout my educational career is a huge contribution of anything I have and ever will achieve in life. She always put my needs in front of her own in order to see me reach my highest potential in life. She demonstrated, by example, what it means to always try your hardest and to never give up. I will never forget the love and support my mother gave me during this significant time of my life.

Acknowledgements

I would like to thank my advisors, Dr. Goswami and Dr. Stefanakos, for their support and guidance throughout my graduate career. I am very grateful to have the opportunity to gain the invaluable research experience of working at the Clean Energy Research Center. I also want to acknowledge my other committee members, Dr. Manoj Ram and Dr. John Kuhn, for their assistance in my research. I also want to acknowledge Dr. Mark Jaroszeski and Dr. Kumar for allowing me to use their equipment.

I would especially like to thank my colleague and doctoral candidate Emre Demirocak. He assisted me throughout every single step of my research and thesis. I simply could not have done any of this without Mr. Demirocak's guidance. He took time out of his schedule for the sole purpose of helping me reach my goals and I greatly appreciate it, those deeds did not go unnoticed. Thank you Emre and I hope the best for your doctorate degree and the rest of your career.

Table of Contents

List of Tables

List of Figures

Abstract

It is of great interest to develop and utilize a high surface area material with optimized hydrogen sorption properties. The need for a renewable energy source to replace automobile gasoline has become more critical in the past decade. Hydrogen is a viable fuel source for automobile usage; however, the question of how hydrogen will be safely and efficiently stored still remains. Critical factors for optimum hydrogen storage include ambient conditions and low activation temperature for adsorption and desorption phenomena. In order for optimum hydrogen adsorption to be achieved, the properties of (1) high surface area, (2) optimum hydrogen adsorption energy, and (3) Kubas interactions between metals and hydrogen molecules need to be considered. Fullerenes have recently become more popular with the discovery and mass production of graphene sheets derived from graphite. Graphene is a modified form of graphite that takes the form of sheets with less agglomeration than its respective graphitic form. This form has the potential for high surface area and storage capabilities. Storage of hydrogen at room temperature must be optimized by increasing the surface area and having an adsorption enthalpy between 15 – 20 KJ/mol. Graphene (G) sheets and graphene oxide (GO) sheets have been utilized as a matrix for hydrogen storage. These materials can also be cross-linked with organic spacers in order to form a porous framework of higher surface area. Metal decorating by calcium and platinum of the G/GO matrix has been used to enhance Kubas interactions, adsorption enthalpies, and spillover phenomenon. The use of a polymer matrix has also been implemented. Polyaniline is a novel superconducting

polymer with unique electronic properties. Complexes of Polyaniline with graphene and graphene oxide have been investigated for hydrogen storage properties. Graphene and graphene oxide surface modification via metal decoration have been investigated in order to determine the most efficient synthesis and particle size on the G/GO matrix. Characterization by XRD, BET, adsorption enthalpy, PCT, TGA, FT-IR, and TEM/SEM (when applicable) were employed to optimize and compare the materials in the effort to develop a suitable storage material.

Chapter 1. Introduction

1.1. Hydrogen – The Need for a Renewable Fuel Source

For the past few decades, the speculation of increasing global temperatures has questioned scientists of the effects of air pollution and toxic emissions. Scientists have been linking elevated global temperatures to the recent increase in category 4 and 5 hurricanes in the Atlantic Ocean [1]. *Science* reports that the strength and duration of hurricanes has increased by 50% in the past 3 decades. Kerry Manual, a professor of atmospheric science at MIT, has a model that estimates an increase of 5% intensity of hurricanes and typhoons for every 1 $^{\circ}$C rise in sea surface temperature [2]. Experts prove that the recent spreading of Malaria and other infectious diseases to never-exposed regions is due to an increase in the global temperature [2]. These effects and others like severe droughts and extinction of animals have been linked to the fluctuations in the global temperature. The planet is seemingly self-destructing with habitats and ecosystems being destroyed everywhere. Sustaining our local environments and ecosystems should be our top priority. If the causes of this global climate crisis can be reduced or prevented all together, then we can further sustain our planet for future generations to come [2].

Fossil fuel consumption through burning coal and gasoline is the main link to the global temperature fluctuations in the recent decades. Figure 1.1 shows the increasing consumption of fossil fuels and the rate of the global temperature [3]. This is only a

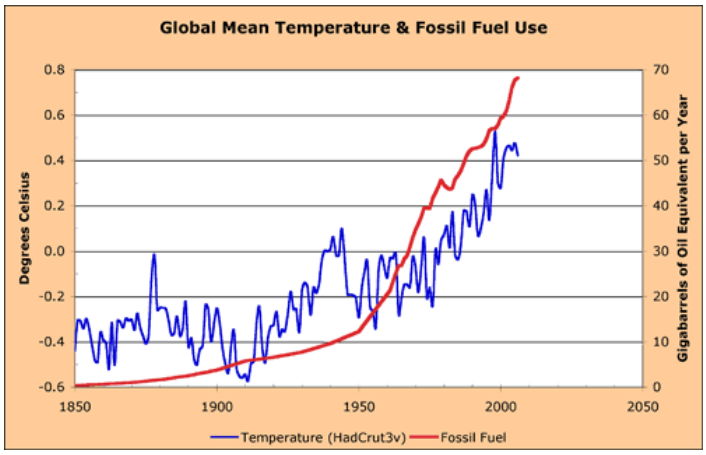

Figure 1.1 Global Mean Temperature (blue) and Fossil Fuel Use (red); Copyright by the Ecological Society of America [3]

correlation and not a direct cause since there are obviously numerous factors that affect the global temperature or some may suspect it is the planet taking its course through time and the temperature change is "natural. [3]" The burning of coal and oil releases toxins such as carbon dioxide and sulfur dioxide into the air which contribute to the greenhouse effect. This effect is characterized by these gases causing the sun's heat to be trapped in our atmosphere causing our planet to warm. The sun's rays are supposed to bounce back to space but with our increasing greenhouse gas emissions they are being re-radiated to the lower atmosphere and heating the Earth like a car in a parking lot on a hot summer's day. These greenhouse gasses include carbon dioxide, nitrous oxide, ozone, chlorofluorocarbons (CFCs), and methane. The most contributing of these is carbon dioxide followed by methane [3]. In order to sustain the earth it is vital to prevent these greenhouse emissions reaching the atmosphere. Investigating the sources of these gases

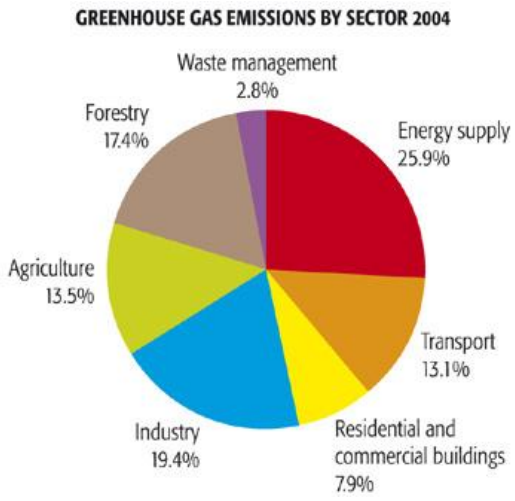

Figure 1.2 Greenhouse Emissions by Sector in 2004; Reprinted (adapted) with permission from *Greenhouse Gas Emission Footprints and Energy Use Benchmarks for Eight U.S. Cities.* Copyright 2012 American Chemical Society [4]

and what economic sector they derive from can be easily shown in figure 2. This figure shows that power stations, industrial processes, and transportation fuels are the top 3 most contributors of greenhouse gases. All of these burn either gasoline or coal. Almost 20% of Carbon dioxide emissions derive from transportation fuels while the rest is from burning of coal for electricity and in industrial processes. By finding a fuel that can be burned instead of coal and gasoline, almost a quarter of the greenhouse emissions can be eliminated [4]. The destruction of the environment to obtain coal and gasoline needs to also be taken into account. Mountain ranges and national parks are being leveled in order to reach coal that is buried deep under the surface. A source of fuel must be used that doesn't require our environment to be destroyed and releases minimal toxins into the atmosphere.

One could deem it necessary to develop a society more dependent on renewable fuel sources for environmental or even political concerns. One can reason that the oil reserves will eventually dry up one day and implementation of another fuel source needs

to be looked at before said day. Experts estimate that the oil reserves have reached their peak and are on the downfall now [5]. It is imperative that a renewable and environmentally-friendly fuel source be researched and developed. A clean-energy fuel source is a source of fuel that emits no greenhouse gases and has no toxic by-products when consumed. Hydrogen is a clean-energy fuel because it can be produced by electrolysis through water, which is abundant in our oceans, and when burned produces no harmful emissions [5].

Hydrogen can be burned in an internal combustion engine or it can be utilized in a fuel cell with oxygen in order to produce electricity and water as its by-products [6]. It has been thought to be a viable fuel source for onboard automobile application. Many automobile companies, such as Honda, BMW, and Volkswagen, have already incorporated hydrogen into the system of their car. Hydrogen can be used as an ignition source in complement with gasoline. However, the internal combustion chamber must be adjusted in order to accommodate the differences of hydrogen over gasoline [6]. Hybrid automobiles have been developed with an increase in miles per gallon due to the high efficiency of burning hydrogen over gasoline [6]. Hydrogen contains about 2.6 times the energy per unit mass of gasoline, but it requires almost four times the volume due to its low density [6]. Hydrogen needs to be charged into an automobile and stored until its time of use. The storage material needs to be reversible and not lose its storage efficiency after numerous charges of hydrogen. The difficulties that arise from this volume dilemma are discussed in the following sections.

1.2. Overview of Current Hydrogen Storage Options

The most challenging aspect of incorporating hydrogen into an automobile's engine is the storing of it until time of use. Other problems consist of producing hydrogen in a low-emission process while also safely storing and handling the gas. The most ideal method to produce hydrogen would be to run electrolysis and split water into oxygen and hydrogen. However, this process requires electricity which needs to may come from a photovoltaic cell or possibly a turbine from a windmill. Once this electricity is produced without the burning of fossil fuels, the hydrogen production process consumes a negligible amount of non-renewable resources [6]. The problem still lies within the issue of safely and efficiently storing hydrogen until its time of use.

Hydrogen is the lightest element and has an extremely low density of 1 kilogram of gas per 11 m^3 along with a high diffusivity [6]. Due to its small atomic size, hydrogen can dissipate through most materials of reasonable thickness; therefore, precautions must be taken to minimize this phenomenon. There are currently five methods of hydrogen storage [6]:

1) High pressure gas cylinders
2) Liquid storage in cryogenic tanks
3) Physical adsorption in high surface materials
4) Chemical absorption in metallic materials
5) Composites of high surface area and metallic materials

The context of the storing of hydrogen for this thesis is on-board automobile storage. The concept is to develop a car that burns only hydrogen gas in an internal combustion chamber. Drivers would need to charge their car with hydrogen which would need to be

stored until time of use. Safety and volume are the most critical factors that one must consider.

1.2.1. High Pressure Cylinder Storage

Hydrogen is most commonly stored as a gas in a high-pressure cylinder. This cylinder must have high-tensile strength to hold up to about 800 bar of pressure [6]. Light-weight materials have been developed to safely store hydrogen in a cylinder at the necessary pressure. Materials require a high tensile strength, low density, inert to hydrogen, and must not allow hydrogen to diffuse through it. Today, many cylinders are made of either austenitic stainless steel or some type of copper alloy [6]. The process of pressurizing hydrogen is commonly performed by a mechanical, piston pump. This method of storage is dangerous because of the pressure requirement and the impracticality of the large cylinder being built inside of an automobile. Dangerous situations arise when considering automobile accidents, explosions, and flammability. Also, the Department of Energy desires to have at least 8 kg of hydrogen in order to drive a car 600 miles. The density of hydrogen at standard temperature and pressure is 0.09 kilogram per cubic meter. Therefore, in order to have 8 kg of hydrogen on-board, one would need a cylinder 88.89 cubic meters large, which would be impractical for on-board automobile storage [7]. Due to the low density of hydrogen in its gaseous phase and the dangerous high pressures of the cylinders, this option is not viable for on-board automobile storage.

1.2.2. Liquid Storage at Cryogenic Temperatures

Hydrogen may also be stored as a liquid at extremely low temperatures commonly called cryogenic temperatures. It must be stored at or below the critical temperature of hydrogen, which is 33 K. To be stored at ambient (room) pressure, hydrogen must be kept at 21.2 K in order to eliminate loss of gas from boil-off. It is estimated that the boil-off rate for a 50 m^3cylinder is 0.4% by volume per day. In order to liquefy hydrogen, the Linde Cycle is implemented with the use of liquid nitrogen to assist the liquefaction cycle [6]. This process is tedious and has a high electrical requirement. Taking into account the high electrical requirement and the inevitable boil-off rate, this method is not desirable for automobile application.

1.2.3. Physical Adsorption in High Surface Area Materials

It is of great interest to develop materials that have the ability to store and release gas at ambient temperature and pressures. Physical adsorption (a.k.a. physisorption) is the phenomenon of gas molecules physically bonding to the surface of the material. The primary forces active in physisorption are weak Van der Waals forces which occur between molecules of like or dissimilar identity. Van der Waals forces, also called intermolecular forces, account for the forces excluding the forces due to covalent bonds, ionic bonds, and electrostatic interactions [8]. The gas molecules interact with two forces of the adsorbent, attractive and repulsive forces. These forces are proportional to the distance the molecule is to the surface of the adsorbent. Due to these weak forces, adsorption only occurs at low temperatures around 298 K when at ambient pressure [9]. The most investigated materials for this type of storage are carbon-containing materials.

These consist of carbon nanotubes, carbon nanowires, fullerenes, graphene, and derivatives of these materials [10]. Aspects that need to be considered for adequate gas storage are the pore size, pore distribution, surface area, and adsorption enthalpy. The adsorption enthalpy is considered to be the interaction energy between the adsorbent and each hydrogen molecule [10]. It is generally assumed that hydrogen only takes part in monolayer adsorption, which is adsorption on the outer surface of the adsorbent. However, the engineering of materials can form microporous structures that allow hydrogen adsorption throughout the layers of the material [6]. At liquid nitrogen temperatures (77 K), the storage of hydrogen is directly proportional to the surface area of the material. However, at room temperatures this may not be true with numerous interactions playing a role in adsorption. The kinetics of this storage option occur very rapidly due to the fact that only weak physical forces are taking part in adsorption. Advantages of this option are the ambient pressure for uptake and release of hydrogen, light-weight material, cost effective material, environmentally friendly, fast kinetics, and facile design of the storage system [6]. Critical disadvantages include the low temperature for adsorption and low gravimetric density of hydrogen on the surface of carbon materials [6].

1.2.4. Chemical Absorption of Metals and Metal Hydrides

Chemical adsorption (a.k.a. chemisorption) refers to the material forming an atomic bond with the absorbing hydrogen molecules. This is a chemical reaction that is occurring, unlike every other storage option which is simply a physical modification of hydrogen [11]. Most chemisorption consists of hydrogen atoms attaching to interstitial

sites of a material. Most commonly, metal hydrides possess interstitial sites that attract hydrogen atoms for chemical bonding. This bonding occurs at room temperature and pressure; however, increased temperature is required to release the hydrogen atoms back into their gaseous phase. The desorption temperature corresponds to the enthalpy of the metal hydride-hydrogen system. The enthalpy measures the stability of the material, yet it needs to be overcome in order to desorb the hydrogen into its molecular phase [6]. It should be noted that the absorbed hydrogen are in their atomic state. Standard desorption temperatures for metal hydride complexes are no lesser than 250 °C. Metal hydrides also oxidize with the atmospheric oxygen and water molecules; therefore, handling of these materials must be done in a nitrogen-rich environment like a glove box. Due to the chemical bonding occurring within the material, the kinetics of the absorption and desorption of hydrogen occur at a slower rate than the other storage options. An advantage is that this storage option has the highest storage density of hydrogen. Disadvantages include the difficulty of handling the material, high activation temperature, and slow kinetics of absorption and releasing of hydrogen [11].

1.2.5. Composite Polymer/Metal Materials

Investigation into this field is becoming increasingly popular in order to engineer a material with specific advantages from each of the materials within the composite. One can look at these composites as a hybrid of materials in order to diminish the disadvantages of a material while magnifying the advantages in order to yield an all-around suitable material for hydrogen storage. Many polymers such as Polyaniline (PANI) and Polypyrrole (PPY) are used as substrates for transition metal and metal

hydride deposition. PANI's unique electronic properties as a conducting polymer have sparked an interest for its use in hydrogen storage [12]. Metal nanoparticles are the most common material to be deposited into a polymer substrate. Extensive research has been performed on polymer-metal complexes to investigate their conducting and electronic properties for uses in microchips and computers [12]. Composites that utilize carbon-containing compounds such as graphene and carbon nanotubes as a substrate for metal deposition are of new interest for hydrogen storage capabilities. The idea is to engineer a hybrid of physisorption and chemisorption materials that complement each other's advantages and disadvantages to yield an ideal storage material.

1.3. Challenges of Hydrogen Storage and Future Goals

Hydrogen has the potential to replace gasoline as an automobile fuel and dramatically reduce the greenhouse gas emissions of the planet. The rewards of such a paradigm shift fuels research groups and government agencies around the world. Once a storage material has been found, then it is necessary to start developing the infrastructure to accommodate the new hydrogen economy. The infrastructure would need to include hydrogen production companies and hydrogen fuelling stations for consumers.

The primary challenge of hydrogen is its storage until its desired time of use by the automobile. As stated previously, storage is difficult due to hydrogen's small molecular size and low density in its gaseous phase. Hydrogen is also extremely reactive as a gas at ambient conditions, which is why it is not stored in its molecular form. The United States Department of Energy (DOE) has taken responsibility of organizing and

implementing goals for research groups to achieve. Criteria that need to be considered for adequate storage are [6]:

1) Gravimetric Hydrogen Storage Capacity
2) Volumetric Hydrogen Storage Capacity
3) Storage Design/Material Cost
4) Fuelling Time/Sorption Kinetics
5) Cycle Life
6) Temperature and Pressure of Delivery

Gravimetric storage capacity is defined as the weight of hydrogen stored in material divided by the total mass of the storage system including the stored hydrogen. The volumetric storage capacity is defined as the mass of stored hydrogen divided by the total volume occupied by the entire storage system. This value is of importance when considering the volume constraint for the placement on an automobile. The material costs needs to be taken into account in order to sell an automobile that is reasonable for the majority of the population to afford to purchase. Fuelling time is critical when thinking about the practicality of consumers using fuelling stations in their daily schedule. It would be unreasonable to develop a material that requires an hour to transfer hydrogen into one's storage tank. Desorption kinetics are also critical when referring to the time to desorb the hydrogen from one's tank into the internal combustion chamber. A quick desorption time allows for a more facile design of the storage system. Cycle life refers to the reusability and reversibility of the storage system to repeatedly store and release hydrogen without losing its efficiency. The pressure and temperature of delivery are important for obvious reasons for the storage system design and safety aspects [13]. DOE

has set goals for until the year 2015 for each of the previous criteria which are shown in the Table 1.1 [13].

Table 1.1 DOE 2015 Targets for Hydrogen Storage Criteria [13]

Storage Criteria	**Units**	**2015**
Gravimetric Capacity	kg H_2 per total kg	0.09
Volumetric Capacity	kg H_2 per L system	0.081
Fuelling Time	min	3
Cycle Life	Cycles	1500
Temperature	°C	[-45,80]
Pressure	atm	100
System Cost	$ per kg H_2 stored	67

The DOE target goals have been estimated assuming the fuel efficiency of hydrogen and the assumed efficiency of available internal combustion chambers suited for the burning of hydrogen. The scope of this thesis will focus on maximizing gravimetric capacity, cycle life, and temperature of delivery.

1.4. Overview of Hydrogen Storage Capacities of Various Materials

This is a very difficult subject to discuss due to the inconsistency of the methods of reporting hydrogen storage and the lack of reproducibility amongst publications. Past publications have reported gravimetric storage capacities ranging from 10 to 20 weight % for Polyaniline and magnesium hydride derivatives, however, those publications have been proven erroneous and therefore invalid; errors derive from the sensitivity of experimental setup and incorrect reporting of units for hydrogen storage capacities. Storage capacities are also reported at various temperatures, for instance at the temperature of liquid nitrogen, 77 K, and can be misleading if one does not take notice. A

brief overview of the achievements of hydrogen storage in each major field of materials is presented in the proceeding sections.

1.4.1. Metal Hydrides for Hydrogen Storage

Utilizing metal hydrides and hydride complexes for hydrogen storage has been the material of choice for the greater part of the past decade. Metal hydrides, specifically magnesium hydride, have the capability of having a storage density of 6.5 H atoms per cm^3 while liquid hydrogen only has a density of 4.2 H atoms per cm^3 [11]. This advantage is promising to reach high gravimetric uptake of hydrogen while maintaining a safe vessel. Metal hydride complexes consisting of lithium, aluminum, beryllium, magnesium, and sodium make up the majority of this class of materials due to their light atomic weight. Hydrogen is absorbed into the material by dissociating on the metal surface and hydrogen atoms are then chemically bonded within the interstitial sites of the lattice complex [11]. The "bottleneck" with this material is the activation energy required to break the interstitial bonds and release the hydrogen atoms from the material. Table 1.1 shows that the maximum temperature set by the DOE is 80 °C. It has been a tedious challenge to lower the temperature below 150 °C for metal hydride complexes [11]. The following table shows storage capacities and desorption temperatures of various metal hydrides that had the highest potential for adequate hydrogen storage.

Table 1.2 Storage Properties of Mg, Na, and Li Hydrides [11]

Material	Desorption Temp. (°C)	Kinetics (min)	Hyd. Storage (wt.%)
MgH_2	300	12.5	7.00
MgH_2 - 2 at.% Ni	200	150	6.50
MgH_2 - 2 at.% Ti	210	3.35	5.00
$NaAlH_4$	90-150	120	5.00
Mg_2Ni	280-330	1	4.10
Li_2NH	255	5	6.50

Table 1.2 proves that metal hydrides have the ability to store high gravimetric amounts of hydrogen, but the temperature to release said hydrogen is always above 150 °C. One must also consider the time of desorption for automobile use. Table 1.2 shows various materials that require an hour or two in order to desorb all of the stored hydrogen. Irreversibility problems also occur with metal hydrides due to their degradation when exposed to compounds such as O_2, CO_2, NO_2, and CO [14]. These compounds are either found in the surrounding atmosphere or produced when hydrogen is burned for fuel. Usually after 100 cycles, the hydrogen storage capacity is dramatically decreased, especially with metal hydrides that contain magnesium due to its strong affinity to oxidize [14]. Various oxide catalysts and transition metals additives have been investigated to improve the cycle life and decrease the desorption temperature. The challenge lies within finding the optimum concentration of catalyst to be added to the metal hydride, while also considering the cost of said catalysts [14]. However, achieving a desorption temperature below the DOE targets still remains a challenge for these types of materials [14].

1.4.2. Porous Organic Polymers for Hydrogen Storage

Organic polymers have been closely studied for hydrogen storage as an answer to the difficulties with metal hydrides. Polymers can overcome the high desorption temperature and kinetics problem simply due to their sole physisorption process of hydrogen. Since only physical adsorption is occurring, no chemical bonds are being formed with the adsorbent and the hydrogen molecule. The weak Van der Waals forces that are taking part can easily be broken to release hydrogen while doing so in an extremely rapid manner for adsorption and desorption [15]. The dilemma for these materials is to engineer a pore size that is adequate to adsorb hydrogen at ambient conditions. The pore size must fall in the microporous region of smaller than 10^{-6} meters in diameter between walls of the pore [16]. Another critical factor is the specific surface area of the material which increases when the pore size decreases [15]. Due to the low adsorption enthalpy of organic polymers, low temperatures (77 K) are required in order to adsorb a reasonable amount of hydrogen, which happens to be the temperature of liquid nitrogen [15]. The specific surface area of a material is also tested at the liquid nitrogen temperature due to the increased accuracy at this temperature. The Brunauer–Emmett–Teller (BET) equation is primarily used with nitrogen adsorption curves in order to evaluate the surface area [16]. This equation will be further discussed in proceeding chapters. Table 1.3 shows various organic polymers with their respective surface area and hydrogen adsorption at 77 K.

Table 1.3 BET SSA and Hydrogen Storage of Organic Polymers [16]

Material	BET Surface Area (m^2/g)	Hyd. Storage (wt.%)
poly(styrene-co-divinylbenzene)	1060	0.80
hypercrosslinked polystyrene	840	1.3
amine-polystyrene	600	1.1
hypercrosslinked plyaniline	426	0.77

Observing the trend in the BET specific surface area (SSA) and hydrogen storage columns, one can see that there is a direct relationship between them. This can only be said at the liquid nitrogen temperature. Room temperature trends are not as consistent due to various interactions occurring within the molecule that are tedious to simulate. The hydrogen storage in Table 1.3 is at 77 K. When room temperature is approached, these values decrease to a range of 0.1 – 0.3 weight % [17]. This is primarily due to the adsorption enthalpy of the material. The adsorption enthalpy of most organic polymer materials range from 4 – 7 KJ/mol, but need to be in the range of 15 – 20 KJ/mol if hydrogen storage at room temperature is desired [15]. The most common method if increasing adsorption enthalpy and hydrogen storage is utilizing the spillover phenomenon. Spillover occurs when a transition metal dissociates hydrogen molecules into their respective atoms which are then either absorbed onto the surface or the pores of the material [15]. The transition metal must be deposited onto the surface of the polymer without decreasing the surface area and blocking pores for hydrogen adsorption. This phenomenon will be further discussed in the proceeding chapters.

1.5. Thesis Outline

Chapter 2 of this thesis will be an overview of the experimental procedures performed in synthesizing the investigated materials. The equipment required for

experimental synthesis and characterization will also be presented. Every characterization technique, including background and principles behind characterization, will also be discussed in detail. Material investigation is divided into three categories:

1) Graphene and graphene oxide cross-linking
2) Graphene and graphene oxide metal doping
3) Polyaniline – graphene/graphene oxide composites

These three directions will be characterized and tested for various relevant hydrogen sorption properties. Chapter 3 will discuss the concepts of cross-linking of graphene and graphene oxide dispersions. Chapter 4 will be a detailed explanation of the concept of metal decorating and results from various metals doped on the surfaces of graphene and graphene oxide complexes. Chapter 5 will discourse the synthesis of Polyaniline – graphene and Polyaniline – graphene oxide complexes and exploring different properties that arise from these complexes. Chapter 6 is an overview and discussion of the results with suggestions of future work.

Chapter 2. Experimental and Characterization Equipment

This chapter introduces all of the instruments and equipment used to synthesize and characterize the investigated materials of this thesis. Detailed synthesis procedures will be discussed for the respective material in their corresponding chapter, only a brief overview will be said here. Background theory and equations are discussed when introducing characterization equipment that is directly related to critical hydrogen storage properties of the materials.

2.1. Synthesis Materials and Equipment

This section will include the purity and company of the critical starting materials used in this thesis. It will also include a brief overview of the instruments utilized to synthesize the various materials and composites.

2.1.1. Materials

Most materials were developed and synthesized in the lab in order to control purity and composition of the material. Basic organic solvents and acids were purchased from either Sigma Aldrich or Thermal Fisher Scientific. Chemicals that are not specified were purchased from Sigma Aldrich and will be specified in the procedures of that synthesis in the respective chapter of the material being synthesized. Table 2.1 shows

materials that were especially critical in the synthesis of the various complexes and composites that encompass this thesis.

Table 2.1 Selected Materials and Chemical Information

Material	Purchased From	Purity/Concentration
Graphene Platelets (15 m^2/g)	Angstrom Materials	0.9900
Graphene Platelets (400-800 m^2/g)	Angstrom Materials	0.9900
Graphene Oxide Dispersion in Water	Angstrom Materials	0.5 weight %
Single Layer GO sheets in Ethanol	ACS Materials	0.9900

The materials listed in Table 2.1 were vital starting materials to synthesize the frameworks of high surface area and the polymer composites that will be discussed in detail in Chapters 3 – 5.

2.1.2. Centrifuge

A compact rotor centrifuge was used during my separation steps of the materials synthesized in this thesis. The centrifuge was from Labnet and the Hermle Z200A model. This model has a maximum speed of 6,000 rotations per minute. A centrifuge separates different components of a solution that have a distinct density difference. The heavier particles are pushed to the sides and bottom of the test tubes by the centripetal acceleration of the rotor. The lighter component, usually the liquid, rises to the top and can then be decanted in order to separate the majority of the phases. Vacuum filtration is usually followed in order to completely remove the liquid from the solid particles. Centrifugation is also used when one wants to confirm a dispersion has been synthesized. If a solid is completely dispersed in a solvent, then centrifugation should not be able to

separate the phases, readily. The following figure shows the centrifuge used for the materials in this research.

Figure 2.1 Labnet Rotary Centrifuge [18]

2.1.3. Nitrogen Atmosphere Glove Box

Various materials and synthesis steps were required to be performed in an oxygen depleted environment. The glove box used was an Innovative Technology System One glove box. The purification was less than 1 parts per million (ppm) of oxygen and water vapor in the glove box's atmosphere. Samples that oxidized easily or hygroscopic were handled in the glove box in order to avoid contamination. Figure 2.1 shows an identical glove box to the one used for this thesis.

Figure 2.2 Innovative Technology System One Glove Box [19]

2.1.4. Bath Sonicator

An ultrasonic bath cleaner from MTI Corporation was required to bath sonicate samples. It is a 40 kilohertz frequency bath sonicator with a 120 voltage power input. The ultrasonic power is 180 Watts. The primary use of this equipment was to disperse graphene and graphene oxide in aqueous and organic solvents in preparation for a reaction. The sonicator uses sound waves to vibrate and evenly mix liquid mixtures. Sonication is the key synthesis step to change graphite into its respective graphene form. This will be elaborated in Chapter 3. Figure 2.2 shows an identical ultrasonic bath sonicator that was used for this thesis.

Figure 2.3 MTI Ultrasonic Bath Sonicator of 40 KHz [20]

2.1.5. Ultrasonic Liquid Processor

Ultra-sonication with the use of a micro-tip probe was required for samples that were more difficult to disperse within the solvent of choice. The ultra-sonicator was purchased from QSonica and is the Sonicator Q500 model. This sonicator is a 500 Watt ultrasonic power with a 20 kilohertz of output frequency. A micro-tip probe was used of 0.8 mm in diameter. Figure 2.3 displays an identical model of the ultra-sonicator used for this thesis [21].

Figure 2.4 QSonica Sonicator Q500 [21]

2.1.6. Solvothermal Synthesis Autoclave

A manufactured autoclave was assembled by Dervis Demirocak at the University of South Florida machine shop. It has an air-tight gasket in order to ensure a pressure build-up is accomplished. The autoclave is made from a grade 316 stainless steel that can withstand high temperatures and pressures. It has the volumetric capacity of 55 mL. The autoclave was used for solvothermal synthesis, which is the placement of a dispersion in an autoclave that is stored in an oven for a long duration of time. The heat and the pressure build-up drive the reaction to occur and prevent evaporation of the solvent from occurring. The following figure is a picture of the autoclave used for these synthesis reactions.

Figure 2.5 Stainless Steel Autocalve Used for Solvothermal Synthesis

2.1.7. Mechanical Ball Milling

Ball milling is used to ensure a powder mixture is homogenous and uniform in nature. The ball mill used was a Fritsch Pulverisette P5 planetary ball mill. The mill contains stainless steel balls that are placed with the powder. The mill rotates in a clockwise fashion while the stainless steel balls collide with the sample due to the

centripetal force. Physical modifications on the sample include reduced grain size, particle size reduction, and increased surface area. Ball milling was used to decrease the particle size of the materials while ensuring a homogenous and well-mixed powder solution was synthesized. The speed of the ball mill was commonly ran at 300 rotations per minute [22]. The following figure shows the ball mill used in this research.

Figure 2.6 Fritsch Pulverisette P5 Planetary Ball Mill [22]

2.2. Structural Characterization Instruments

The following instruments were utilized in the structural characterization of the materials developed in this research project. This includes determining the various phases and compounds present in a specific material. Brief background and theory will be discussed with an emphasis on the instruments that are more critical in determining the hydrogen sorption properties of the material.

2.2.1. Fourier Transform – Infrared Spectroscopy (FT-IR)

Fourier Transform – Infrared Spectroscopy is an important and facile instrument used to detect certain organic functionality groups detectable in most materials. The theory behind the instrument is that an infrared beam passes through the material and interference is measured by an interferometer. The pattern received by the interferometer is then translated back to a spectrum by a Fourier transform. This spectrum shows specific peaks at wavelengths of infrared light. The measured property is percent transmittance of light through the material. When the percent transmittance is affected at specific wavelengths (a.k.a. wavenumbers), a peak is shown on the spectrum. This peak can be correlated to a specific bind of the molecule [23]. Each type of bond, for example a carbon-oxygen or a carbon-nitrogen, yields a signal at a distinct wavenumber. FT-IR can prove whether a specific compound is found in a material by either the presence or absence of said compound's characteristic peaks on the spectrum [23]. FT-IR will be utilized to confirm polymerization of aniline, cross-linking of graphene oxide, and extent of metal decorating on graphene and graphene oxide. A Perkin Elmer Spectrum One was the spectrometer used for all FT-IR tests in this thesis. The following figure shows this model of FT-IR used.

Figure 2.7 Spectrum One FT-IR Spectrometer [23]

2.2.2. X-Ray Diffraction

X-Ray Diffraction (XRD) is a method of characterization that aims to determine the crystal structure of the material. XRD is a critical method of investigation of a product that can determine if the correct phases are present in the sample. It is usually only used for crystalline compounds; however, it can shed some light on the structure of an amorphous compound. XRD was used, in some occasions, to compare samples of Polyaniline with Graphene and Graphene oxide complexes. A Philips X'Pert X-Ray diffractometer was used for all powder XRD analysis. Figure 2.8 shows the XRD instrument used in this research. It is implied from this point on in the thesis that XRD refers to powder X-ray Diffraction. Sample preparation is performed by pelletizing the powder sample and using double-sided tape to mount the pellet on an inert Silicon disc that is then placed in the wall mount of the XRD instrument.

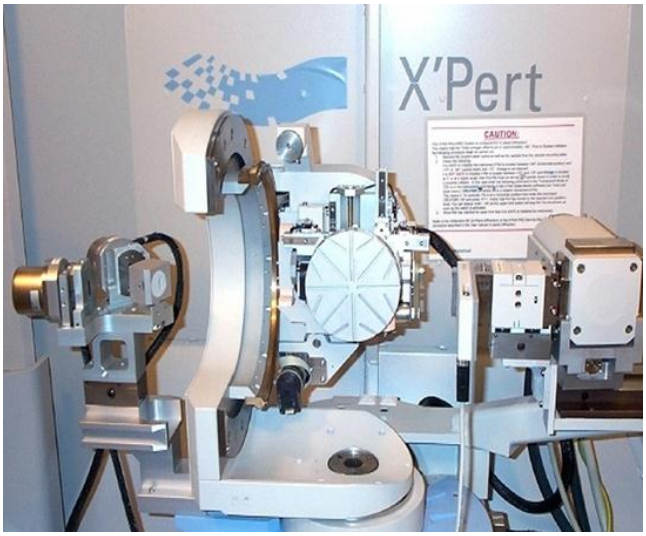

Figure 2.8 Philips X'Pert X-Ray Diffractometer [24]

XRD has the potential to determine the chemical composition and physical characteristics of the sample. Examples of physical characteristics include grain/particle size and lattice formation [25]. The principle behind the XRD instrument is based on the idea that X-rays have constructive, or diffracted, interference when directed at the atoms of a sample. This diffraction of X-rays can be modeled by Bragg's law, which is the following equation [25]:

$$n\lambda = 2d\,sin\,\vartheta \qquad 2.1$$

Where n is the order of the X-rays, λ is the corresponding wavelength of the X-ray, d is the interlayer spacing between the planes of the atomic crystal, and θ is the angle of incident of the X-ray [25]. By utilizing Equation 2.1, one can determine the interlayer spacing and crystal structure of a given sample. The XRD instrument operates by a beam rotating around the sample at various 2θ angles with a receiver rotating to capture the diffracted beams. When the directed beam heats an atom in the crystal lattice, it causes a diffraction that follows Bragg's law. The diffracted beams cause a spike in the signal of

the plot that correlates to a specific crystal phase. Interpreting these peaks can help identify the phases present and the composition of the sample. Figure 2.9 shows an X-ray beam diffracted by atoms in the crystal lattice of the sample.

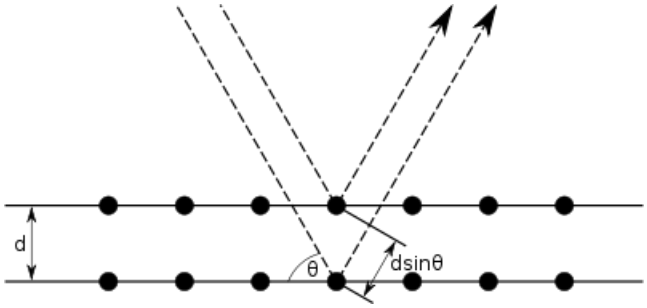

Figure 2.9 X-ray Diffraction Causing a Signal Peak [25]

The Scherrer equation can also be applied to an XRD plot in order to determine particle size (grains size) and number of layers in a sample. The Scherrer equation is:

$$\tau = \frac{K\lambda}{\beta \cos \vartheta} \qquad 2.2$$

Where τ is the mean size of the particle, β is the line broadening at half the intensity, λ is the wavelength of the X-ray, and θ is the Bragg angle from equation 2.1 [25]. The Scherrer equation is only valid for nano-scale particles and its accuracy depends on the broadness of the signal from the XRD plot; error increases as the peaks become broader [25]. It is important to note that this equation yields a lower bound on the particle size due to various factors that contribute to the broadening of a peak. The Scherrer equation was used to determine the number of graphene layers present and the size of metal particles deposited on polymer and graphene complexes.

2.2.3. Scanning Electron Microscopy (SEM)

Scanning Electron Microscopy can play a vital role in the structural characterization of a material. It is useful in determining the surface morphology, or physical structure and texture, of a material. Surface morphology affects the material in a variety of ways. SEM works by directing a beam of electrons directly at the surface of a material to bombard the electrons off the superficial layer electrons [26]. Electrons called secondary electrons are ejected from the k-orbitals due to inelastic scattering of the material and captured by an electron detector [26]. This electron detector transmits an output of a two-dimensional display. Limitations of SEM occur because one can only view the top layer of the material. Surface properties such as grain size, particle distribution, particle size, crystal defects, and crystal formation can be viewed by an SEM. It was mostly used to determine the particle distribution of the metal doped complexes along with the size of the metal particles on the surface [26]. A Hitachi S800 Scanning Electron Microscope was used for the analysis of all samples in this thesis. The figure below shows the SEM instrument used in this research.

Figure 2.10 Hitachi S800 SEM Used for Surface Analysis [24]

2.2.4. Specific Surface Area Tests

Determining the specific surface area is the most important factor in evaluating the hydrogen storage potential of a physisorption material. In 1938, Stephen Brunauer, Paul Hugh Emmett, and Edward Teller published a theory about physical adsorption of surfaces. It was coined the term "BET" theory derived from the first initial of their last names. BET theory extended from the Langmuir surface area theory which only explained monolayer adsorption of a material. Langmuir equation relates the surface coverage, or adsorption, of gas molecules to the relative pressure applied to the adsorptive. BET theory models monolayer and multilayer adsorption of a material. They basically assumed there was no interaction between the layers of the material, in which they could apply the Langmuir method to each layer of an infinite amount of layers in a material [16].

BET and Langmuir utilize the adsorption isotherm of a material and applies a specific equation to determine the specific surface area (SSA). The isotherm is a measure of the volume of gas adsorbed at constant temperature as a function of the gas pressure. Adsorption is performed with nitrogen as the adsorptive which results in adsorption at the liquid nitrogen temperature of 77 K. At this low temperature, molecular interactions are minimized and the nitrogen is able to absorb and desorb into the pores of a material with ease. The modeling of this remains simple because of the lack of interactions occurring at this low temperature [16]. Adsorption isotherms can be analyzed and the sample can be categorized into three different classes of porosity [27]:

1) Microporous (< 2 nm)

2) Mesoporous (2 – 50 nm)

3) Macroporous (> 50 nm)

The figure below shows the various types of adsorption isotherms that characterize materials of the three porosities.

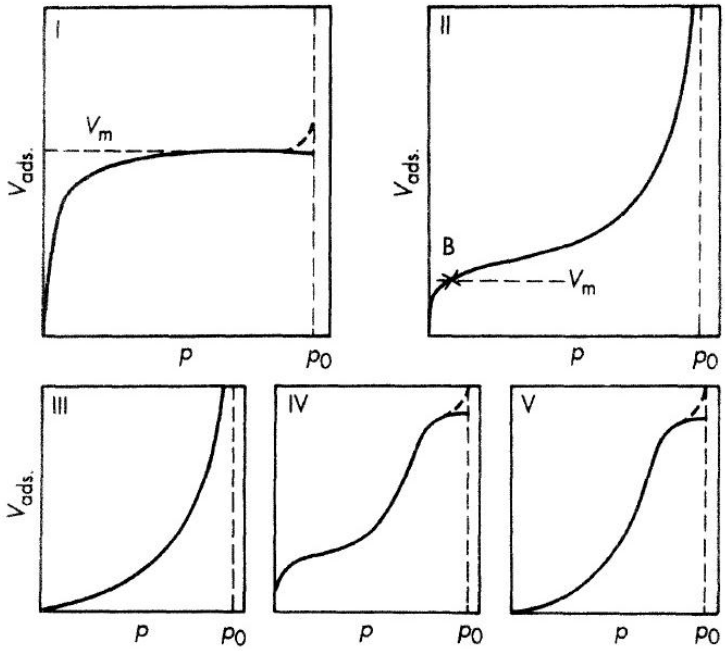

Figure 2.11 Adsorption Isotherms of Types I – V; Reprinted (adapted) with permission from *Introduction to Colloid and Surface Chemistry*. Copyright 2012 American Chemical Society [27]

The V_{ads} is the volume of gas adsorbed into the material and ρ and ρ_0 are the pressure and saturation pressure, respectively. Type I curves are classified as a Langmuir adsorption and is characteristic of microporous materials with only monolayer adsorption occurring. Type II adsorption is characteristic of nonporous or macroporous materials that adsorb monolayer and multilayer coverage. Point "B" on this curve indicates the point of monolayer saturation. Adsorption after this point is within the material's multilayers. This isotherm exhibits reversibility of adsorption and desorption. Type IV

adsorption corresponds to mesoporous materials with multilayer adsorption. These are the primary adsorption curves that appear for the materials in this thesis. Hysteresis occurs when the desorption curve does not follow the same path as the adsorption curve. This occurs when mesopores are present in the material. Hysteresis also yields information about the specific pore shape of the material. The figure below shows an example of hysteresis in a Type IV adsorption isotherm [27].

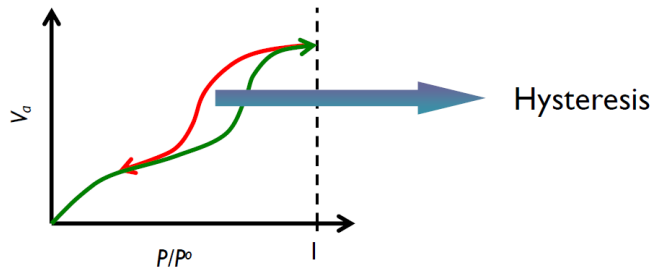

Figure 2.12 Hysteresis Shown in a Type IV Adsorption Isotherm [27]

BET theory uses the below equations to relate the adsorption isotherm of a material with the surface area [9].

$$\frac{1}{v\left[(P_0/P)-1\right]} = \frac{c-1}{v_m c}\left(\frac{P}{P_0}\right) + \frac{1}{v_m c} \qquad 2.3$$

Where c is a constant equal to [9]:

$$c = \exp\left(\frac{E_1 - E_L}{RT}\right) \qquad 2.4$$

Where P is the equilibrium pressure, P_0 is the saturation pressure, υ is the volume of adsorbed gas, υ_m is the volume of adsorbed gas in the monolayer of the surface, E_1 is the adsorption enthalpy of the first layer of coverage, E_L is the adsorption of liquefaction of the material, R is the gas constant, and T is the temperature of adsorption [9]. The BET

equation is only applied in the relative pressure range of $0.05 < P/P_0 < 0.35$ [9]. The specific surface area can then be calculated by the equation below [9].

$$S_{BET} = \frac{v_m N}{V * a} \qquad 2.5$$

In equation 2.5, the N is Avogadro's number, V is the molar volume of the adsorbate gas, and a is the mass of adsorbent. The method of experimentation is using a setup illustrated in the below figure.

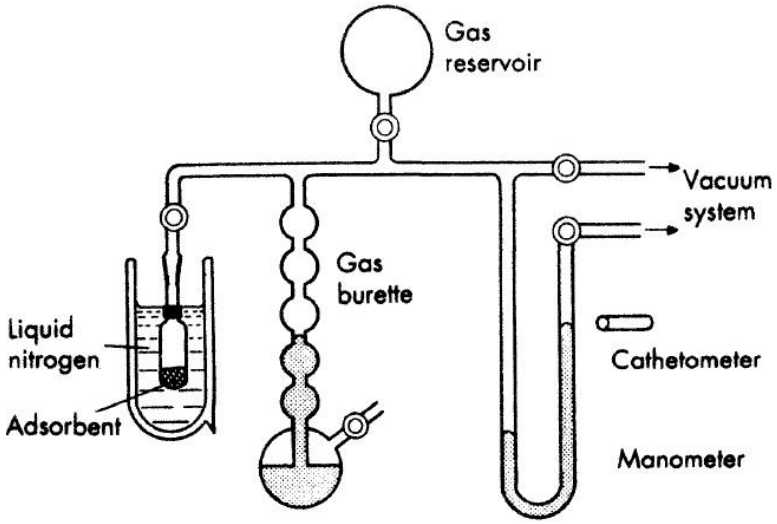

Figure 2.13 Volumetric Apparatus for Gas Adsorption; Reprinted (adapted) with permission from *Introduction to Colloid and Surface Chemistry*. Copyright 2012 American Chemical Society [27]

Specified volume reservoirs are used to record the drop in pressure between the sample and the system in order to extrapolate the volume of gas adsorbed [27]. Equations of states can be used to relate the pressure change to the volume of gas adsorbed. The instrument used for this analysis is the Autosorb1 (AS1) developed by Quantachrome. It also has two outgassing stations with jacketed heaters in order to evaporate all impurities from a sample before it is analyzed. The figure below is an identical model of the

Autosorb 1 used for all BET and gas adsorption experiments at cryogenic temperatures for this research.

Figure 2.14 Autosorb1 BET/Gas Adsorption Instrument [28]

AS1 is also capable of performing hydrogen storage tests at liquid nitrogen levels by using hydrogen as an adsorbate instead of nitrogen. One can also determine adsorption enthalpies of a material by running gas adsorption at liquid nitrogen (77 K) and liquid argon (87 K). Manipulation of equations such as the Clausius – Clapeyron equation can be implemented to find the heats of adsorption (a.k.a. adsorption enthalpy) of a given material [6]. Detailed methods of calculation will be presented in Chapter 3. Micropore analysis and Thermal Programmed Desorption (TPD) are also capabilities of Quantachrome's AS1.

Calibration of Autosorb1 is critical due to the high sensitivity and inherent errors of measuring gas adsorption. Possible sources of error are leaks, pressure sensors, volume errors, and pseudo-adsorption from within the instrument. The instrument was measured

to ensure correct nitrogen and hydrogen adsorption for surface area and hydrogen storage measurements. The material that was used for the calibration test was activated carbon G-60 bought from Norit, which has an established and well-reported surface area of 850 m^2/g [29]. Autosorb1 reported a surface area of 836 m^2/g, which is precise when taking into account the accuracy of the instrument. The hydrogen storage capacity of Norit G-60 activated carbon at 77 K is shown in figure 2.15. The saturation capacity of activated carbon was found to be at about 1.4 weight %, which correlates with literature values for the same material [9].

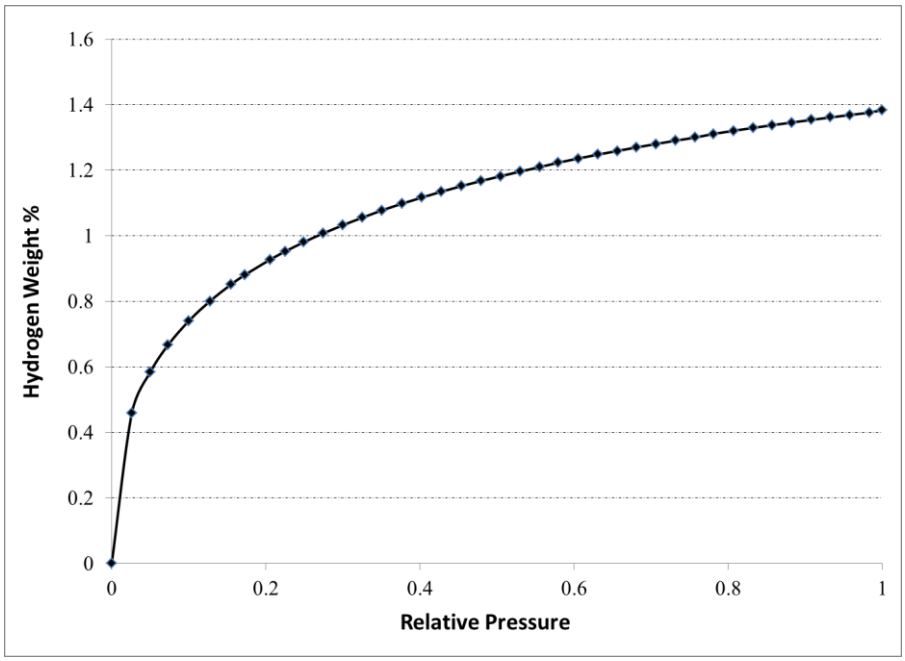

Figure 2.15 H_2 Storage of AC at 77 K

2.2.5. Hydrogen Sorption Test

Hydrogen sorption capacities were tested on the polymer and graphene based samples using the HyEnergy PCT Pro 2000. Gas adsorption is typically measured by either a gravimetric system or a volumetric system. The gravimetric system utilizes

extremely sensitive mass balances in order to determine the increase or decrease in weight of the sample. The PCT Pro 2000 utilizes the volumetric method to measure gas adsorption. This method capitalizes on an accurate volume measurement of reservoirs that are in equilibrium with the sample holder. When the sample absorbs or desorbs hydrogen, the pressure will decrease or increase, respectively. This pressure change can be correlated through the Van der Waal's equation of state to determine the amount of gas stored or released. The Van der Waal's equation is as follows [8]:

$$\left(p + \frac{n^2 a}{V^2}\right)(V - nb) = nRT \qquad 2.6$$

In the above equation, p is the pressure, V is the volume of the container holding the sample, R is the gas constant 8.314 J/mol*K), T is the temperature of the sample in Kelvin, n is the number of moles of gas adsorbed or released, a is the repulsion force between two molecules (0.02476 m^6Pa/mol^2), and b is the volume occupied by a mole of hydrogen molecules (2.661 * 10^5 m^3) [8]. This equation is a modified form of the ideal gas law in order to support the non-ideal conditions of hydrogen storage at high pressures of 80 bar. PCT Pro 2000 directly measures the temperature (T) and pressure (p) of a sample, while a, b, and R are constants throughout the duration of the experiment. Therefore, the number of moles of hydrogen absorbed, n, can be determined. By multiplying the number of moles of hydrogen by its molecular weight of 1.0079 g/mol, the mass of hydrogen stored can be found, labeled as $m_{hydrogen}$. The weight percentage of hydrogen is found by the following equation:

$$Weight\ \% = \frac{m_{hydrogen}}{m_{hydrogen} + m_{sample}} * 100\% \qquad 2.7$$

In literature, there has been some confusion with the definition of hydrogen weight percentage stored. For the remained of this thesis, equation 2.7 is the concrete definition of hydrogen stored in a material. All values will be reported in this form.

The Pressure-Composition Test (PCT) is capable of being run at 500 °C via a heater jacket on the outside of the sample holder. The PCT was operated up to a maximum pressure of 100 bar, due to cylinder restrictions and safety precautions. Purging of the system and sample holder was done with helium before every experiment. Hydrogen leak tests were also performed in order to ensure only a negligible amount of hydrogen was leaking from the holder and system. The figure below is the instrument used for this research [24].

Figure 2.16 HyEnergy PCT Pro 2000 Gas Sorption Instrument [24]

The PCT instrument is capable of two distinct hydrogen sorption tests. The first test is called a kinetics test. This test is fairly simple in it exposes the sample holder containing the material to a specified pressure of hydrogen gas for an extended amount of

time. This test is usually run to determine the time for a sample to become saturated with hydrogen and this is considered the equilibrium time. For physisorption materials, this saturation time should be fairly quick, on the magnitude of minutes. The figure below is an example of a kinetics run on a Polyaniline (Pani) – Graphene oxide (GO) complex at 70 bar of hydrogen pressure. Weight percentage of hydrogen stored is measured as a function of time. Cycles may also be run to determine the reversibility of the given material.

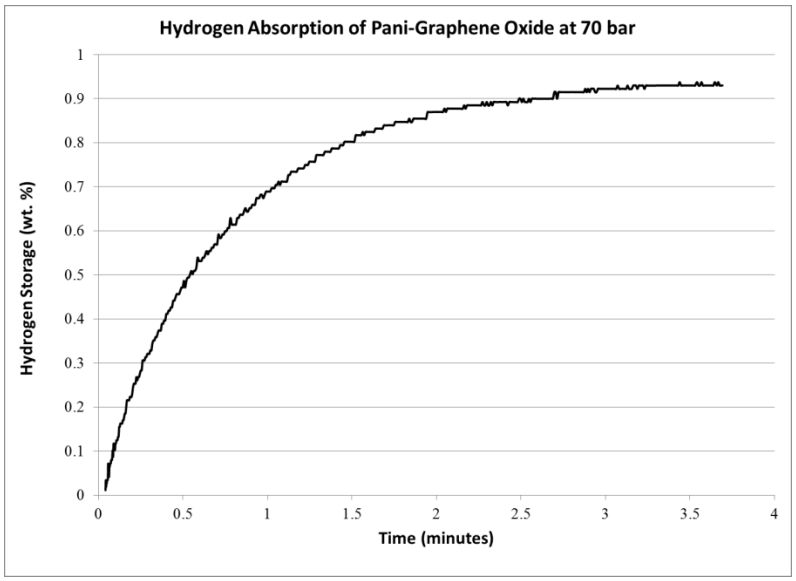

Figure 2.17 Kinetics Plot of Pani-GO at 70 Bar

The second test is a true pressure-composition test (PCT). This test involves exposing the sample to amounts of hydrogen at time intervals of increasing pressure. The time interval is set to reach equilibrium before the next pressure step is exposed to the sample. This time interval can be determined by running the kinetics test. Weight percentage of hydrogen is measured as a function of the applied pressure of hydrogen. Hydrogen uptake and release can be measured by PCT and analysis can be performed in order to determine if complete desorption of the sample occurred and at what pressure is

the sample reached its saturation for hydrogen uptake. Cycles can also be run to determine reversibility of hydrogen uptake and release of the sample. The figure below is an example of a PCT plot of Graphene oxide doped with Calcium.

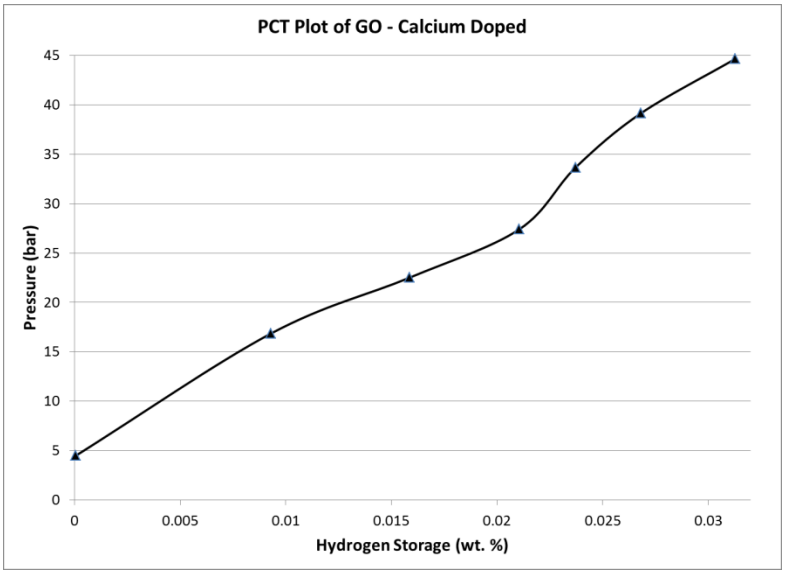

Figure 2.18 PCT Plot of GO Doped with Calcium

2.3. Thermal Characterization

Thermal characterization deals with a materials behavior when exposed to various levels of heat. The only method of thermal characterization used in this research was Thermal Gravimetric Analysis.

2.3.1. Thermal Gravimetric Analysis (TGA)

TGA is an instrument primarily used to measure the thermal stability of various materials up to temperatures around 1000 °C. The TGA instrument used was a Thermal Analysis SDT (Simultaneous DSC and TGA) Q600 shown in the figure below.

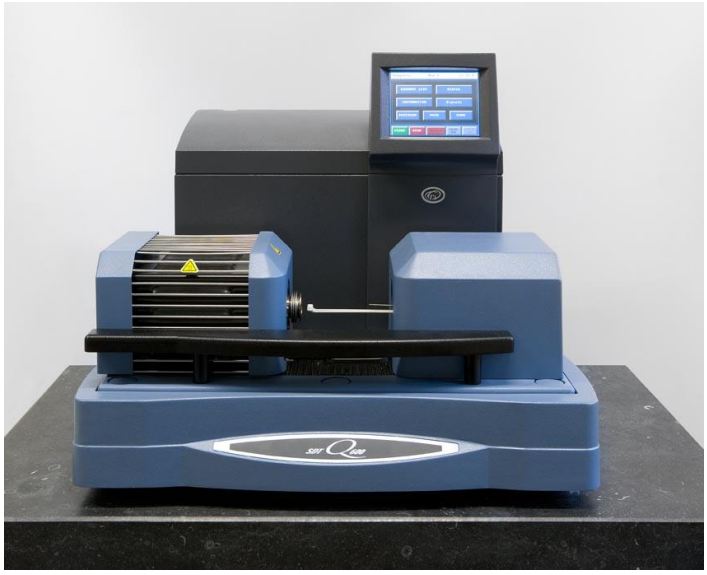

Figure 2.19 Thermal Analysis SDT Q600 Instrument [4]

Thermal stability of all materials was measured before synthesis reactions were performed in order to determine the material's stability throughout the reaction. TGA has an extremely sensitive weight balance to measure changes in mass as a function of increasing temperature. The sensitivity of the instrument is ± 0.1 μg with a temperature limit of 1500 °C [4]. A heating rate of 1 °C/min was employed in order to ensure thermal equilibrium was reached within the sample. The TGA is placed inside of an inert nitrogen glove box to ensure minimal impurities affect the sample. In this thesis, TGA was used to verify thermal stability and to investigate at what temperatures caused a release of hydrogen from the material.

Chapter 3. Graphene – Based Complexes for Hydrogen Storage

3.1. Introduction

This chapter will discuss the hydrogen storage properties of graphene and graphene-based complexes. The primary substrate of these complexes is graphene and graphene oxide. Modification of graphene (G) and graphene oxide (GO) will be performed to optimize the hydrogen storage properties. Methods of modification include cross-linking of the material and metal doping using earth metals and transition metals.

Graphene has become increasingly popular since the first isolation by a physicist at the University of Manchester, Andre Geim, via micromechanical cleavage. Graphene can be simplified to a single layer or isolated atomic layer of the more common carbon allotrope graphite. Andre Geim would end up winning the Nobel Prize in Physics in 2010 for his synthesis and characterization of the novel compound that would boom an explosion of research on graphene and its applications [30].

Graphene is known as the thinnest material in the world with being one atom thick. It consists of two-dimensional (2D) monolayers of sp^2 hybridized carbon in a hexagonal lattice. The six-membered lattice resembles a "honeycomb" that can best be described as "atomic-scale chicken wire. [31]" Figure 3.1 shows the hexagonal crystal lattice that a layer of graphene takes shape.

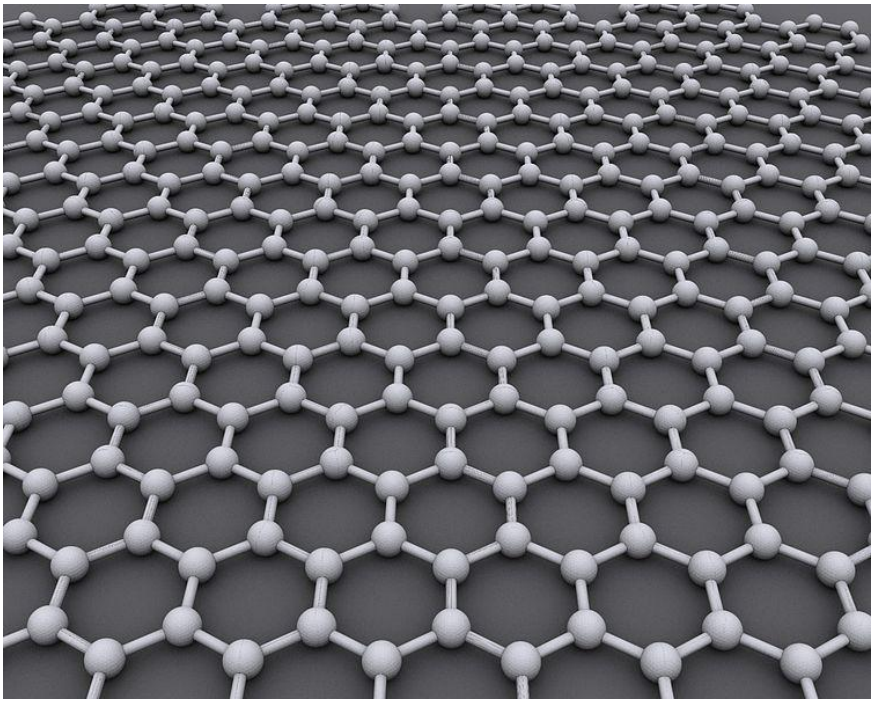

Figure 3.1 Hexagonal Crystal Lattice of a Single Layer of Graphene [31]

Graphite takes form due to layers of graphene stacked around each other in a three-dimensional (3D) framework. When this framework is separated into a flat 2D network of layers, then graphene is developed. Graphene is the only 2D framework composed of only carbon. Graphene is considered to be an allotrope, which is a compound of the same elemental identity but with a different structural framework. Allotropes of graphene consist of diamond (3D tetrahedral lattice formation), graphite, (3D hexagonal lattice), nanotubes (1D formation), and fullerenes (zero-dimensional network) [30]. Graphene has been the allotrope that has attracted the most research and attention from scientists in the past decade [31].

Graphene has attracted most of its attention due to its unique electrical conductivity and optical properties. Its applications include supercapacitors, batteries, nanocomposites, and sensors [30]. The unique electronic properties of graphene derive

from its electrons “obeying linear dispersion relation, yet behave like massless relativistic particles. [32]” This rare occurrence of electronic properties behaves like a hybrid of dense matter and quantum electrodynamics [31]. Some of the rare electronic properties displayed by graphene are the absence of localization and the anomalous quantum Hall effect [32]. Graphene sheets are the building blocks for many compounds including charcoal and graphite. The interlayer spacing between each graphene sheet in graphite is 0.335 nanometers [8]. Graphene has the potential to be a high surface area material due to its inherit spacing between each layer [32].

Hydrogen storage occurs in graphene through physical adsorption, or physisorption. Physisorption is the adsorption of a gas molecule to the surface and within the pores of the complex. Forces involved with physisorption are primarily weak Van der Waals forces that attract and repel the gas adsorbate. These weak forces allow for fast loading and unloading of hydrogen in the material. However, only a small amount of hydrogen is stored at room temperature due to the weak adsorption enthalpies of the material and the hydrogen molecules. Because of this, the parameters that dominate hydrogen sorption are high surface area and optimal pore size distribution [33]. Carbon materials that include carbon nanotubes (CNTs) and metal organic frameworks (MOFs) have also been of extensive interest for hydrogen storage. However, these materials still fall short of the DOE targets for hydrogen storage due to factors of pore size and adsorption enthalpy at room temperature [33]. Graphene can be applied to hydrogen storage by modification of the framework and optimizing the pore size distribution of the complex. Modification techniques such as cross-linking and doping of the structure with metals can optimize adsorption enthalpies, pore size, and surface area of the complex.

Graphene oxide is also of some importance due to its influential oxygen functionalities that may play an important role in hydrogen sorption. The oxygen functionalities also allow this form of graphene to be dispersed in various solvents that may be immiscible for graphene. Graphene and graphene oxide are considered to be zero-gap semiconductors with fast electron mobility compared to its allotropes [32]. Graphene oxide is also utilized as a synthesis route for a feasible method to synthesize graphene. Both G and GO will be investigated for their hydrogen sorption properties.

3.2. Graphene Oxide Production

Graphene oxide is a critical material in this research due to is incorporation in almost every material synthesis. Graphene oxide will be the starting material for the synthesis of graphene and any other derivative of graphene. It has been decided that the synthesis route to form graphene will be to first synthesis graphene oxide then perform a reduction yielding a reduced form of graphene oxide, or simply graphene. Graphene oxide has also been investigated for gas adsorption in the past decade. It has potential to store gas if the surface area can be increased within the structure. The oxygen functionalities on the structure also allow graphene oxide to be easily dispersed in aqueous and organic solvents. This is important in synthesis in order for the graphene oxide to fully take part in the reaction it needs to be fully dispersed throughout the solvent. Figure 3.2 shows the proposed structure of graphene oxide. One can see the carbonyl (C=O), hydroxyl (-OH), ether (R-C-R), epoxy (C-O-C), and carboxyl (R-COOH) groups present throughout the structure. Graphene oxide and graphene will be

compared to each other for their surface area and storage capabilities after various modification techniques will be experimented on the materials.

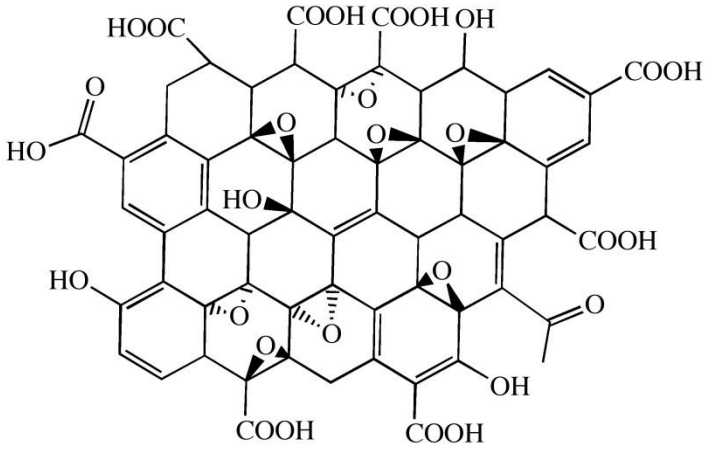

Figure 3.2 Graphene Oxide Structure

3.2.1. Synthesis of Graphene Oxide

Graphene oxide will be synthesized using a well-documented modified Hummer's method. The Hummer's method is simply a synthesis route for complete oxidation of a material. The oxidizing agents used can vary from one research group to another. The oxidizing agents used in the modified Hummer's method are potassium permanganate and hydrogen peroxide [34]. All synthesis materials were purchased from Sigma Aldrich, unless specified otherwise. Synthesis starting materials are graphite powder (<45 μm), potassium permanganate ($KMnO_4$), 30% hydrogen peroxide (H_2O_2), and concentrated sulfuric acid (H_2SO_4). 10 grams of graphite is stirred in 230 mL of sulfuric acid while this flask is kept in an ice bath to remain temperature of reaction around 0 °C. Then 30 grams of potassium permanganate is slowly and carefully added to the mixture while the temperature is kept below 20 °C. This solution is then stirred and once returned to 0 °C,

the ice bath is then removed from the reaction flask. The flask is allowed to cool to room temperature and stirred for 15 minutes. 250 mL of deionized water (DI) is slowly and carefully added to cool the reaction below 98 °C. The reaction is then left to stir for another 15 minutes before being diluting even more by roughly 1 Liter of DI water. Then 100 mL of hydrogen peroxide are added to the solution and then left to stir for 24 hours. The solution is separated by centrifugation at 5000 rotations per minute (rpm) for 30 minutes using a Labnet rotary centrifuge. Vacuum filtration was then used along with excessive rinsing of the filtered product with water to remove unreacted graphite. The filter used is a Whatman qualitative grade 2 (8 μm) filter paper. Outgassing in an oil bath at 80 °C for 24 hours was implemented to yield a finished product of graphene oxide [34]. This is the entire process of the modified Hummer's method to yield graphene oxide. This process was sometimes down-scaled and the correct molar ratios of graphite, potassium permanganate, and hydrogen peroxide were kept constant.

3.2.2. FT-IR Characterization of Graphene Oxide

Fourier Transform Infrared spectroscopy (FT-IR) was utilized to ensure complete oxidation of the graphene was successfully performed. Specific functionalities of carbonyl and hydroxyl groups should be present in the product. Figure 3.3 shows the FT-IR spectrum of the graphene oxide product.

Figure 3.3 FT-IR of Graphene Oxide via Hummer's Method

The peaks at 1624 cm^{-1} and 3400 cm^{-1} are signals showing the stretching and bending of the prevalent O – H (hydroxyl) groups in the product. The signal band at 1725 cm^{-1} is characteristic of the carbonyl groups (C=O) found in the carboxylic groups of graphene oxide. The bands at 1220 cm^{-1} and 1400 cm^{-1} correspond to the hydroxyl and epoxy groups, respectively. This spectrum confirms successful oxidation of graphite to graphene oxide according to the presence of specific signals and its similarity to literature results.

3.2.3. X-Ray Diffraction Characterization

X-ray diffraction (XRD) was utilized to confirm the results of FT-IR in order to ensure graphene oxide was synthesized and no impurity phases are present in the compound. The most prevalent phase will be a graphitic phases that is still present within

the graphene oxide compound. XRD will be able to express the degree of this impurity graphitic phase in the synthesized product. Figure 3.4 shows the XRD pattern of graphene oxide.

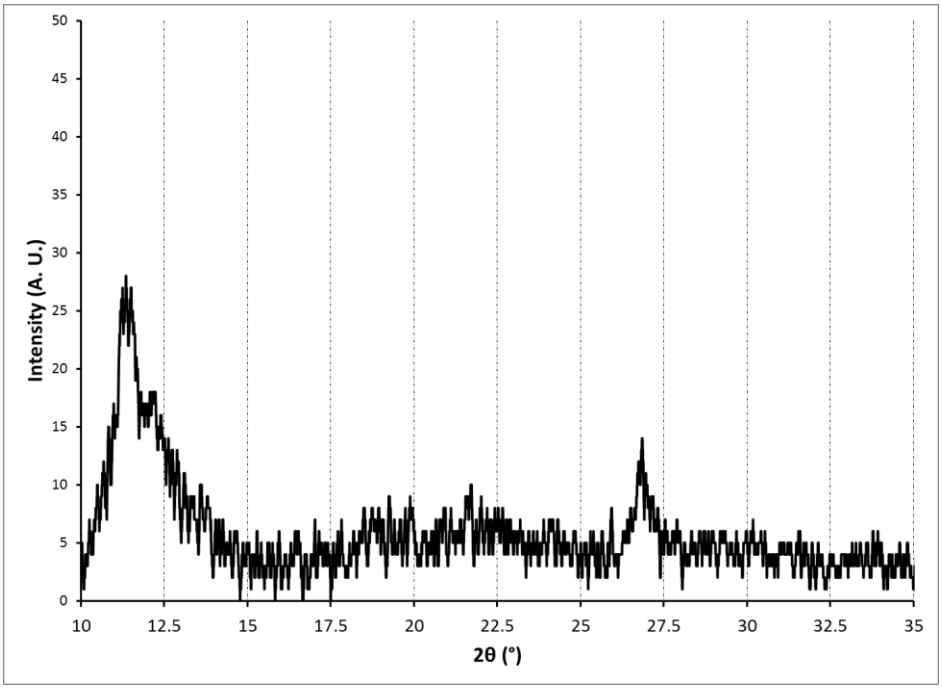

Figure 3.4 XRD of Graphene Oxide

The peaks present are found at about 11 2θ° and 27 2θ°. The peak at 11 2θ° is the dominant peak and corresponds to the (001) lattice point of the graphene oxide phase. This peak shows lattice spacing of about 8.4 Å. This should be the only phase present. The peak at 27 2θ° is characteristic of the graphitic phase of graphite oxide. The intensity of this peak is 1/3 in intensity as the graphene oxide peak. This shows promise of a majority phase of graphene oxide in the product from the modified Hummer's method.

3.2.4. Thermal Gravimetric Analysis

Thermal stability of graphene oxide was measured by Thermal Analysis SDT Q600 in an inert nitrogen environment. The purpose of this measurement is to determine at what temperatures it is safe to handle graphene oxide without undesired reactions occurring in the structure. Figure 3.5 shows the TGA plot of graphene oxide up to the temperature of 500 °C.

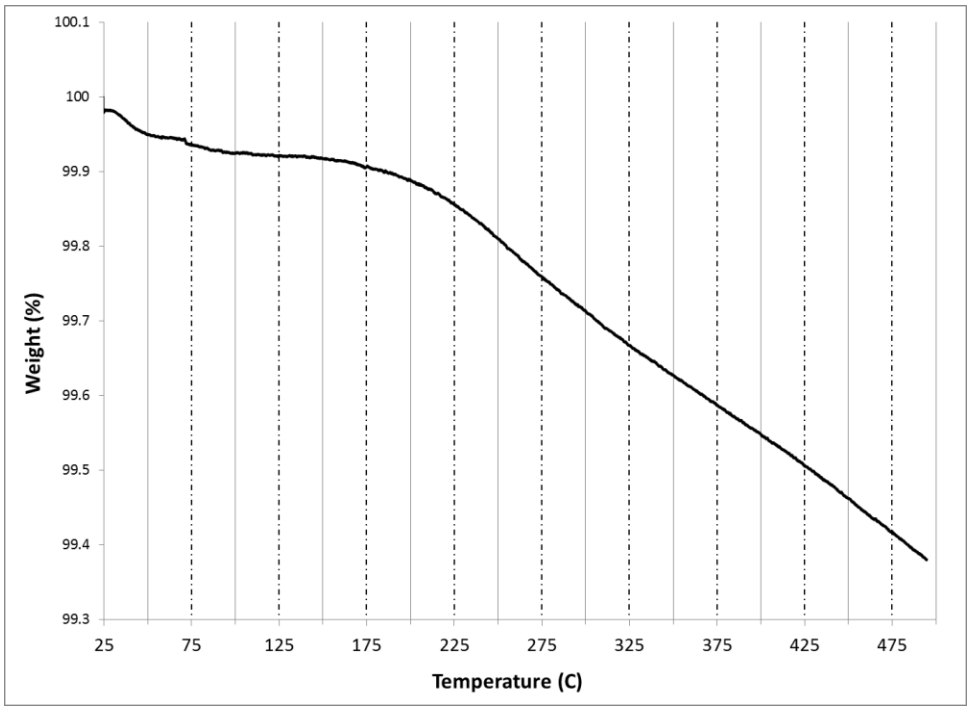

Figure 3.5 TGA Plot of Graphene Oxide

Figure 3.5 proves that graphene oxide is stable up until the temperature of 175 °C. It is not until then that the complex begins to experience weight loss due to undesired reactions within the sample. This temperature will be recorded and it will be noted that reaction and outgassing temperatures should not exceed 150 °C, just to be sure the

integrity of our sample is not compromised. This constraint will also apply for graphene as reported in literature [35].

3.2.5. Surface Area and H_2 Sorption Characterization

Surface area and hydrogen storage measurements were run in order to obtain control results to compare with results after modification of graphene oxide. Surface area was calculated through Autosorb1 instrument and incorporation of BET theory. The surface area was determined to be 18.8 m^2/g. Hydrogen sorption measurements were tested at liquid nitrogen temperature (77 K) and ambient pressure conditions. Figure 3.6 shows the hydrogen capacity of graphene oxide to be at a saturation of 0.18 weight %.

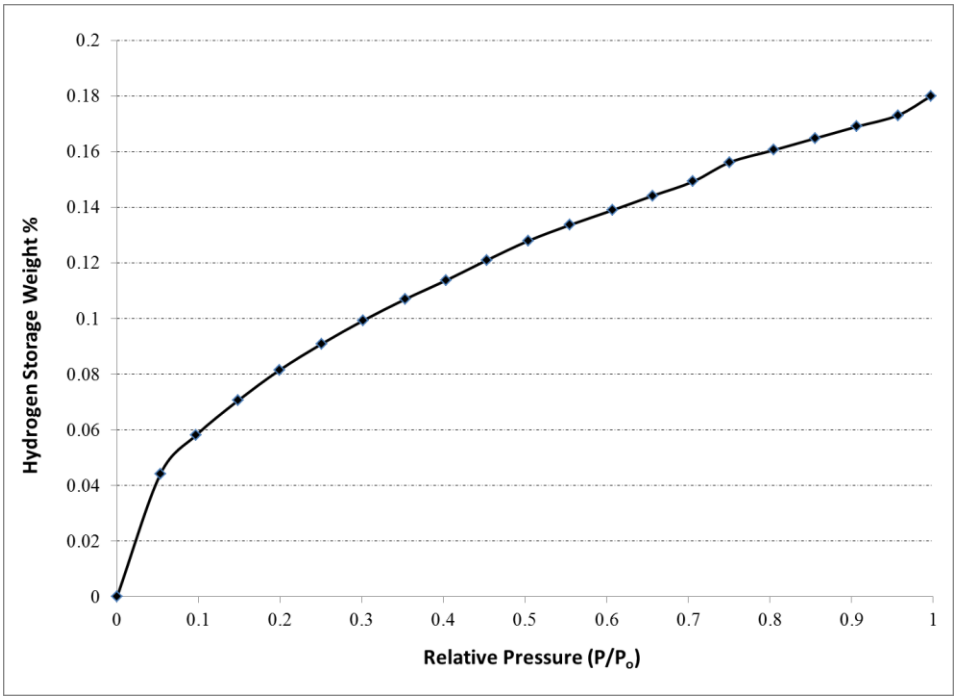

Figure 3.6 H_2 Storage of Graphene Oxide at 77 K

3.2.6. Summary of Graphene Oxide

Graphene oxide was synthesized using a modified Hummer's method in order to completely oxidize graphite and form a product that can be dispersed into various solvents. The dispersion will be beneficial because the graphene oxide will maintain its interlayer spacing between the sheets, which defines graphene oxide different than graphite oxide. FT-IR results shows the according oxygen groups present in the product. XRD also shows a majority phase of graphene oxide over the graphitic phase. Hydrogen storage at 77 K is 0.18 weight %, which translates to a negligible amount of storage at room temperature. This storage capacity will be increased by various methods of modification in this thesis.

3.3. Reduced Graphene Oxide

Many methods of synthesizing graphene have been developed and optimizing since the discovery of graphene. The mechanical cleavage process that was first used to discover graphene is a process that only yields an extremely small amount of graphene per synthesis process and is considered impractical [31]. Graphene sheets were also discovered to be developed via single-crystal silicon carbide via vacuum graphitization. This process had the advantage of being able to directly fabricate the pattern of graphene sheets that was desired for the application. This was a practical approach for electronic applications but tedious for applications that require bulk production at a low cost [10]. Chemical vapor deposition has also been a proven method to synthesis graphene, yet due to equipment cost and product yield, this is an unreasonable route for graphene production. A "wet" chemistry route was desired to synthesize graphene with minimal

defects and aggregation of sheets. A critical problem occurs when graphene sheets are separated from the respective dispersion solvent that is holding it; the sheets immediately stack upon each other and severely decrease the surface area of the complex. Methods to prevent this consist of ultrasonication, cross-linking spacers, and thermal exfoliation treatment [31].

A "wet" chemistry route to reduce graphene oxide into graphene sheets with minimal defects has been developed with variations by different research groups [36], [37]. These variations usually occur with the choice of the reducing agent. A vital requirement of the process is to form reduced GO (rGO) that is dispersible in a variety of solvents. This is important in the doping or cross-linking process where the graphene must dissolve in the solvent in order to take part in the reaction. It is usually recommended that synthesized graphene is dispersible in water and common organic solvents such as ethanol and methanol. Long-term stability in the solvents is usually investigated to determine if the graphene remains a homogenous solution in the solvent or if the particles collect at the bottom proving a colloidal suspension was made, not a dispersion solution. Ultrasonication and bath sonication are both utilized to disperse the graphene oxide and graphene throughout the synthesis process. Synthesis routes were first developed using strong reducing agents like hydrazine, but have since been improved to avoid such toxic and explosive chemicals. Two methods of reduction was investigated and compared in this research; reduction via L-Ascorbic acid and reduction via N,N-dimethylhydrazine.

3.3.1. Synthesis Route via L-Ascorbic Acid

Solution-based chemical routes for the reduction of graphene oxide are the most cost effective and feasible processes to perform for mass production of graphene. Using a mild reducing agent, like L-Ascorbic acid (LAA), prevents harsh reaction conditions and minimizes chemical damage to the complex. LAA is nontoxic and most commonly used for the reduction of living systems that require sensitive treatment. This synthesis route also prevents the irreversible aggregation of the graphene sheets that are undesirable. In this process, the oxidized product of LAA also acts as a capping agent to stabilize the reduced graphene oxide (rGO) product, which also eliminates the need for a capping agent or surfactant [37].

Reduction of the graphene oxide only required a one step, one pot chemical synthesis. L-Ascorbic acid was the only chemical required. The synthesis begins with dispersing the graphene oxide, synthesized by the modified Hummer's method as stated in section 3.2, into DI water. The concentration of the aqueous GO dispersion is 1 mg/mL. The aqueous dispersion of GO is performed by ultrasonicating 1 mg of GO powder in 100 mL of DI water for 30 minutes. Ultrasonication was performed by a QSonica Sonicator Q500. The dispersion was then centrifuged to remove excess GO particles that were not dispersed in the DI water. The dispersion was then left over night to ensure the GO particles were sufficiently dispersed in the DI water.

The reduction procedure was to place 1.00 g of L-Ascorbic acid in 100 mL of aqueous GO dispersion (1 mg/mL). This mixture is vigorously stirred for 48 hours before complete reduction is performed. Separation is performed by vacuum filtration then the

sample is outgassed in an oil bath at 80 °C for 24 hours [37]. The filter used is a Whatman qualitative grade 2 (8 μm) filter paper.

3.3.2. FT-IR Characterization of LAA Reduction

Fourier Transform Infrared Spectroscopy was performed on the sample in order to verify the reduction was successfully performed on graphene oxide. FT-IR was performed measuring the % transmittance of the sample. Sample was prepared by mixing in potassium bromide powder and then pelletizing. Figure 3.7 shows the FT-IR spectrum of the reduced GO product from the reduction process via L-Ascorbic acid.

Figure 3.7 FT-IR Spectrum of rGO via L-Ascorbic Acid

The oxygen – containing functionalities that characterize graphene oxide are shown in Table 3.1 with their respective signal wavelength. One expects to see most of these signals reduced or disappear after the chemical reduction process.

Table 3.1 FT-IR Chart of Oxygen Functionalities of rGO via LAA

Oxygen Functionality	Wavenumber (cm^{-1})	Analysis
C = O	1726 cm^{-1}	Slightly weakened
O – H	3395 cm^{-1}	Still Present
O – H	1410 cm^{-1}	Slightly weakened
C – O (epoxy)	1226 cm^{-1}	Disappeared
C – O (alkoxy)	1052 cm^{-1}	Disappeared

By examining the FT-IR spectrum, it appears that 4 out of 5 of the oxygen-containing signals either weakened or completely disappeared after the reduction using L-Ascorbic acid.

3.3.3 Synthesis Route via N,N-Dimethylhydrazine

Reduction of graphene oxide was also attempted using N,N-dimethylhydrazine (DMH) as the reducing agent. The graphene oxide was dispersed in N,N-dimethylformamide (DMF) because literature reports that this solvent is optimal for the graphene oxide to be sufficiently reduced [28]. The theory behind this synthesis is the fact that graphite can easily be oxidized to graphite oxide which can then be dispersed and exfoliated in a solvent. Once the dispersion has been considered to be long-term stable in the solvent, it can then be reduced, or deoxygenated, to form electrically conductive graphene [28]. This is the facile synthesis route for the reduction of graphene oxide in any dispersion using an ultrasonicator and modified Hummer's method.

The synthesis starting materials are graphite (<45 μm), N,N-dimethylformamide (DMF), and N,N-dimethylhydrazine (DMH). The graphene oxide dispersion in DMF is prepared first and tested for long-term stability. Graphene oxide is prepared via the modified Hummer's method as stated in section 3.2.1. A solution of 0.5 mg/mL of concentration is prepared of GO in DMF. In this instance, 200 mL of the GO dispersion was prepared, which amounts to 100 mg of GO dispersed in the solution. This solution was dispersed via ultrasonication using the QSonica Sonicator Q500 for 30 minutes. The solution is then vigorously stirred and placed in a water bath at 95 °C. Then 130 mg of DMH (1.3 mg per 1 mg of GO) is slowly added to the solution and stirred for 1 hour. One should notice the color of the solution turn from a dark grey to a rich black color. Separation was performed by vacuum filtration and outgassed in an oil bath at 80 °C for 24 hours before any testing was performed on the sample. The filter used is a Whatman qualitative grade 2 (8 μm) filter paper.

3.3.4. FT-IR Characterization of DMH Reduction

Fourier Transform Infrared Spectroscopy was performed on the sample to measure the % transmittance of the pelletized powder sample of reduced graphene oxide via DMH. The oxygen-containing functionalities are being investigated to consider if complete reduction was performed on the graphene oxide sample. Figure 3.8 shows the corresponding spectrum for the reduced graphene oxide sample via DMH in the solvent DMF.

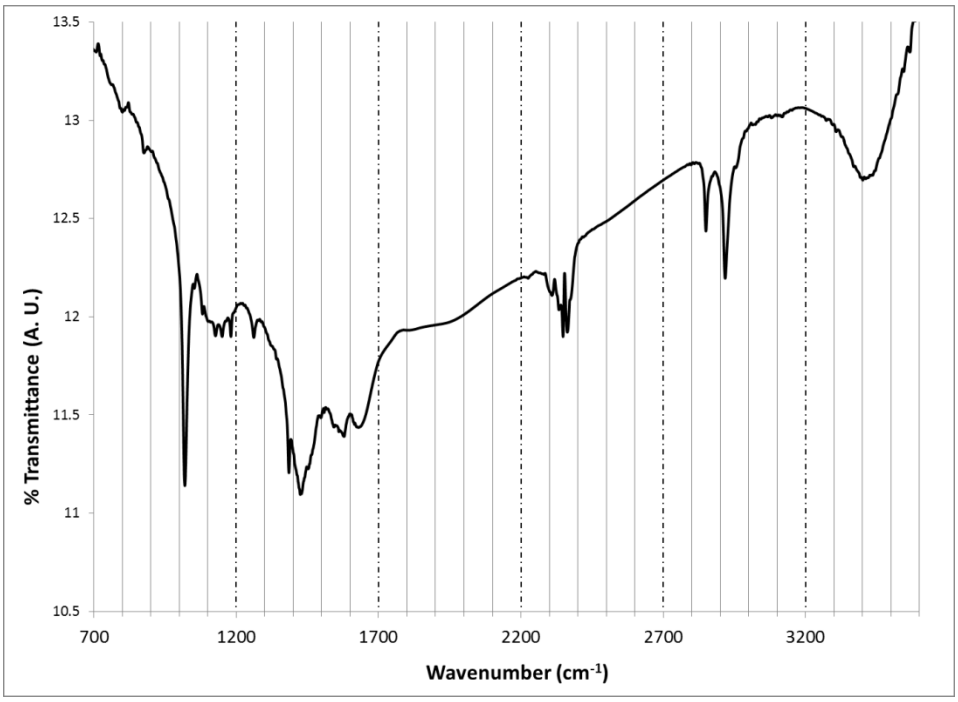

Figure 3.8 FT-IR Spectrum of rGO via DMH

The analysis of the oxygen-containing functionalities is shown in the table below. One would expect for the majority of the oxygen signals to either weaken or disappear completely.

Table 3.2 FT-IR Chart of Oxygen Functionalities of rGO via DMH

Oxygen Functionality	**Wavenumber (cm^{-1})**	**Analysis**
C = O	1726 cm^{-1}	Disappeared
O – H	3395 cm^{-1}	Still Present
O – H	1410 cm^{-1}	Slightly weakened
C – O (epoxy)	1226 cm^{-1}	Disappeared
C – O (alkoxy)	1052 cm^{-1}	Disappeared

3.3.5. Summary of Results

The products of both reduction processes were compared to each other to determine which process successfully reduced graphene oxide to graphene. The following figure compares the FT-IR spectrum of graphene oxide before reduction and both products of each reduction synthesis.

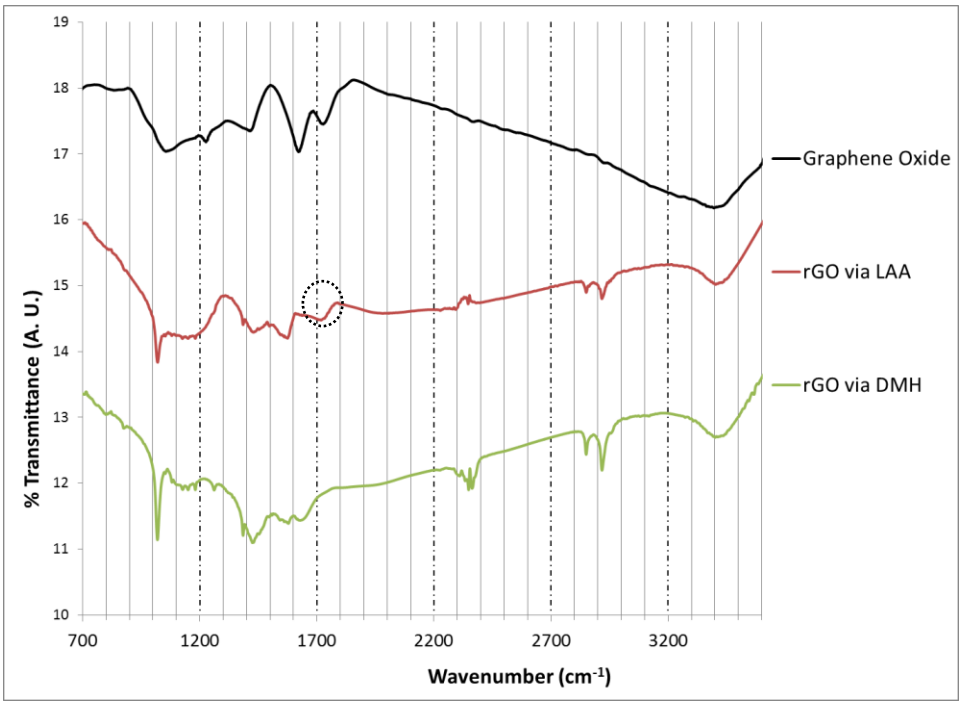

Figure 3.9 FT-IR Comparison of GO, rGO via LAA, and rGO via DMH

The only difference between the reduced graphene oxide products is the absence of the signal at 1726 cm^{-1} for rGO via DMH. Figure 3.9 shows a circle around the peak that rGO via LAA contains that shows it wasn't completely reduced. This signal corresponds to the carbonyl (C=O) group of the graphene oxide structure. In conclusion, the reduction using N,N-dimethylhydrazine (DMH) of graphene oxide to graphene is the

preferred synthesis and will be utilized in other parts of this research when graphene is required as the starting material.

3.4. Calcium Doping of Graphene and Graphene Oxide

Metal doping of graphene and graphene oxide aims to optimize the adsorption enthalpy of the hydrogen molecules with the storage material. Adsorption enthalpy measures the attraction of hydrogen molecules to the surface of the adsorbent. It is the single most important property to characterize the surface chemistry of physisorption materials. Adsorption enthalpy in the range of 1 – 10 kJ/mol of H_2 is ideal for storage at liquid nitrogen (77 K) temperature. It is desired to increase the enthalpy to the range of 15 – 20 kJ/mol of H_2 to increase the storage of hydrogen at room temperature [38]. One way to achieve this increase in enthalpy is to dope the surface with a transition metal such as titanium or platinum. The transition metal binds with hydrogen molecules through hybridization of the hydrogen molecule and the anti-boding orbital with the d-orbital of the transition metal; this phenomenon is called Kubas interactions [38]. The difficulty in his process is the tendency of transition metals to cluster on the surface of nanomaterials instead of being evenly dispersed. This occurs due to the high cohesive energy (4 eV) of transition metals [38].

The other alternative to optimize the adsorption enthalpy is the doping of carbon structures with alkali and alkali earth metals, for example lithium, potassium and sodium. The most promising of these metals is considered to be calcium (Ca). Calcium has a much lower cohesive energy of only 1.8 eV, which minimizes clustering on the surface of the nanomaterial [38]. Dr. Stephen G. Louie and his research group at University of

California – Berkley have determined, through various theoretical Monte Carlo simulations based on density functional theory, that calcium has the potential to store 8 or 9 weight % of hydrogen at room temperature [38]. This group simulates that each calcium atom can bind up to six hydrogen molecules with an ideal binding energy of 15 kJ/mol [38]. This holds much promise if a synthesis route can be developed to sufficiently dope carbon nanomaterials.

3.4.1. Synthesis of Calcium Doped Graphene and Graphene Oxide

Problems arise in determining a chemical synthesis route to sufficiently dope the surface of graphene and graphene oxide with calcium atoms of minimal clustering. A synthesis route was developed and modeled after a chemical reduction process using metal precursors added to a G or GO dispersion. More specifically, this process was modeled after a process to dope carbon materials with transition metals using metallic acids as precursors. Starting materials required are calcium chloride hexahydrate, 3-(N,N-dimethyldodecylammonio) propanesulfonate (SB12), sodium carbonate, dilute (1 M) sulfuric acid, and aqueous dispersions of graphene and graphene oxide. The ratio of calcium to carbon atoms for both G and GO synthesis was determined to be 4:14 by Dr. Louie's research group [38]. This ratio was utilized to determine correct mass ratios for all chemicals. First, 101.30 mg of calcium chloride hexahydrate is dissolved into 10 mL of DI water. This solution is neutralized to a pH of 7 via sodium carbonate. Then the calcium solution is added into an aqueous dispersion of graphene or graphene oxide. For graphene, 20 mg of graphene is ultrasonicated for 30 minutes in 40 mL of DI water. For graphene oxide, 17.54 mg of graphene oxide is ultrasonicated for 30 minutes in 40 mL of

DI water. Then the calcium – graphene/graphene oxide solution is neutralized to a pH of 7 via sodium carbonate. 39 mg of the surfactant, SB12, in 12.5 g of methanol is then added to the solution and the solution is vigorously stirred and kept at 80 °C for 90 minutes. A few drops of dilute (1 M) sulfuric acid are then dropped into the solution in order to precipitate the Ca – graphene or Ca – graphene oxide compound. Vacuum filtration with rinsing by methanol and DI water is repeatedly done to remove unreacted particles from the product. The filter used is a Whatman qualitative grade 2 (8 μm) filter paper. Outgassing at 80 °C for 25 hours is performed in an oil bath before characterization is performed.

3.4.2. FT-IR Characterization of G – Ca and GO – Ca

Characterization is performed by Fourier Transform Infrared spectroscopy in order to analyze the compounds before and after doping with calcium. The calcium doped products should not show any newly formed bonds on the infrared spectrum since Ca bonds do not produce a signal. If new bonds are formed, then an impurity phase has been produced by the calcium doping. Figure 3.10 compares the spectrum of graphene from Angstrom Materials and the graphene doped with calcium.

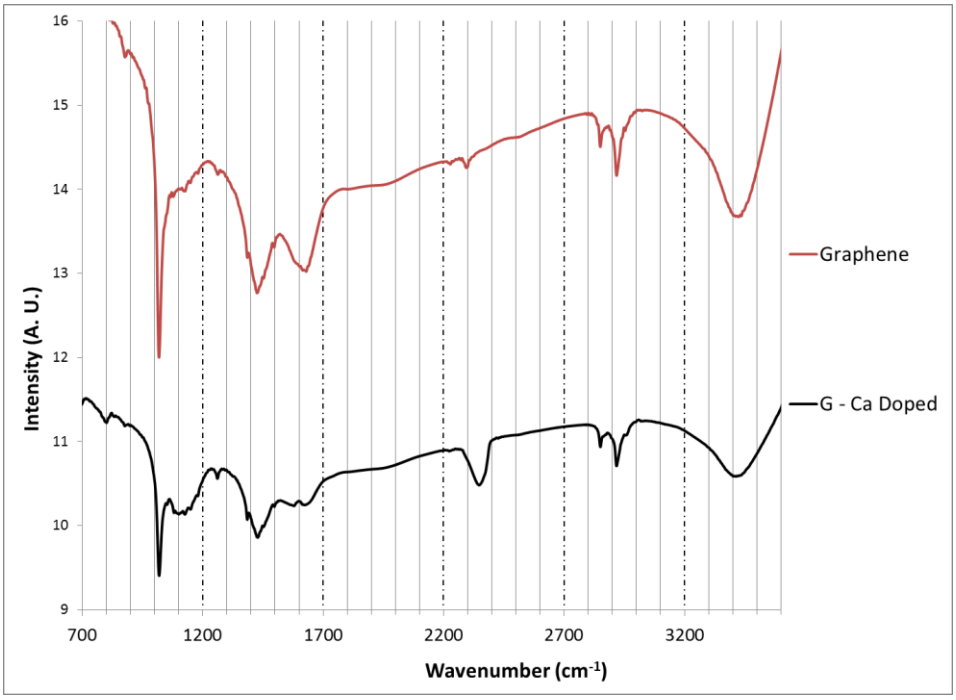

Figure 3.10 FT-IR Spectra of Graphene and G – Ca Doped

Peaks at 1650 cm^{-1} and 1120 cm^{-1} appear to weaken and sharpen, respectively, in the graphene doped with calcium product. This may be due to calcium clustering over certain areas of graphene's carbon bonds that cause this difference in peak intensity.

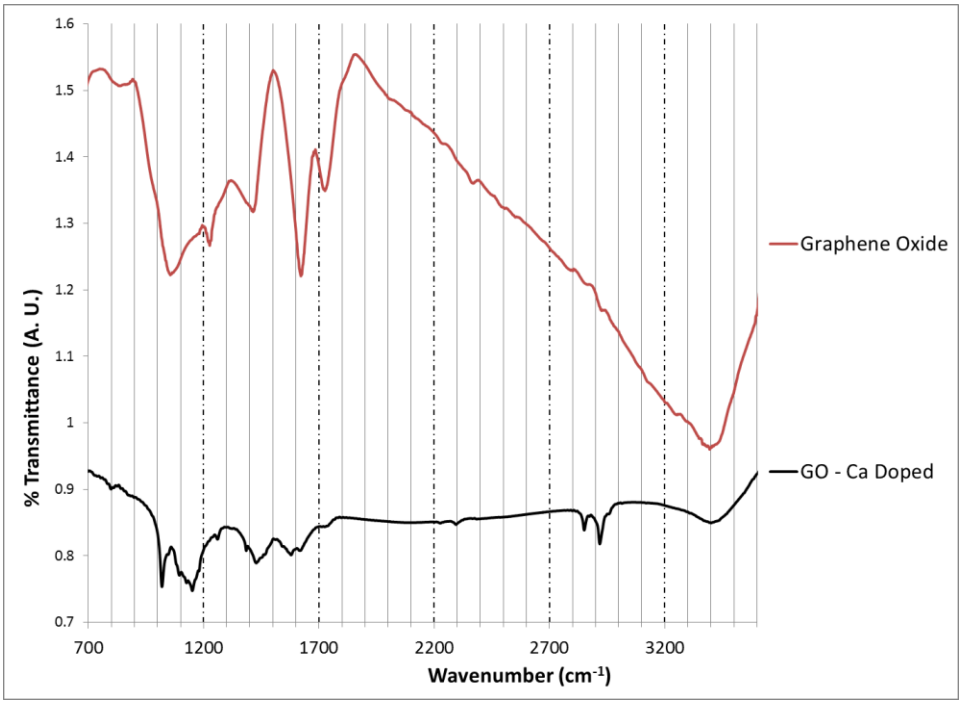

Figure 3.11 FT-IR Spectra of GO and GO – Ca

Figure 3.11 compares the spectra of graphene oxide, synthesized via Hummer's method, and graphene oxide doped with calcium. There is a strong weakening of the signal at 1710 cm^{-1} which corresponds to the carbonyl group of graphene oxide. This weakening may be due to calcium clustering around localized areas of the graphene oxide surface that inhibit detection by the infrared spectroscopy. It appears that both calcium doped forms of graphene and graphene oxide are synthesized with minimal impurity phases present in the lattice.

3.4.3. Surface Area Characterization

Surface area tests were performed on both doped samples of G and GO using the Autosorb1 instrument. Mass samples in the range of 100 – 200 mg were loaded into the

instrument for testing. The nitrogen adsorption plots for graphene – calcium and graphene oxide – calcium are shown below in Figure 3.12.

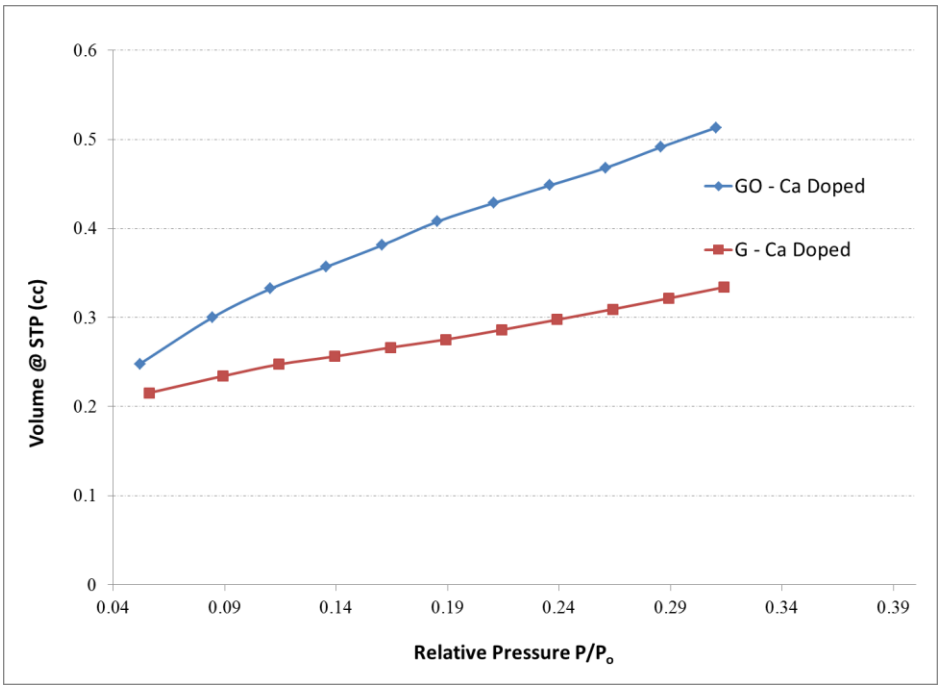

Figure 3.12 BET N_2 Adsorption Plot of G – Ca and GO – Ca

Both 11 point N_2 adsorption plots are inserted into Equation 2.3, the BET equation, in order to evaluate the specific surface area of each material. The calculated specific surface area was determined to be 8.41 m^2/g and 8.15 m^2/g for G – Ca and GO – Ca, respectively. These values correlate with a degree of clustering of calcium atoms that either fill surface pores or aggregate on the surface of the material. Table 3.3 shows a comparison between untreated and doped complexes of graphene and graphene oxide.

Table 3.3 BET of Untreated and Doped G and GO

Sample Name	BET SSA (m^2/g)
Graphene Oxide	18.8
Graphene	11.3
GO – Ca	8.2
G – Ca	8.4

3.4.4. H_2 Sorption Measurements at 77 K

Hydrogen sorption tests were run for both calcium doped samples using Autosorb1 at 77 K. This test will show a direct relationship of surface area to storage capacity of hydrogen. This relationship is only proportional when testing at the liquid nitrogen temperature. The storage at 77 K gives one an idea of what room temperature storage capacity should be. This can only be estimated when dealing with physisorption materials. It is estimated that every 1000 m^2/g of surface area adsorbs 1 weight % of hydrogen at 77 K [16]. Figure 3.13 shows the hydrogen adsorption of calcium doped graphene and graphene oxide at 77 K. The maximum storage of G – Ca and GO – Ca doped is 0.01 wt. %, and 0.0045 wt. %, respectively. It appears that graphene is a more suitable complex to store hydrogen when doped with calcium. This may be due to graphene's lack of oxygen functionalities that impede or reject the adsorption of hydrogen molecules on the surface of the carbon sheets.

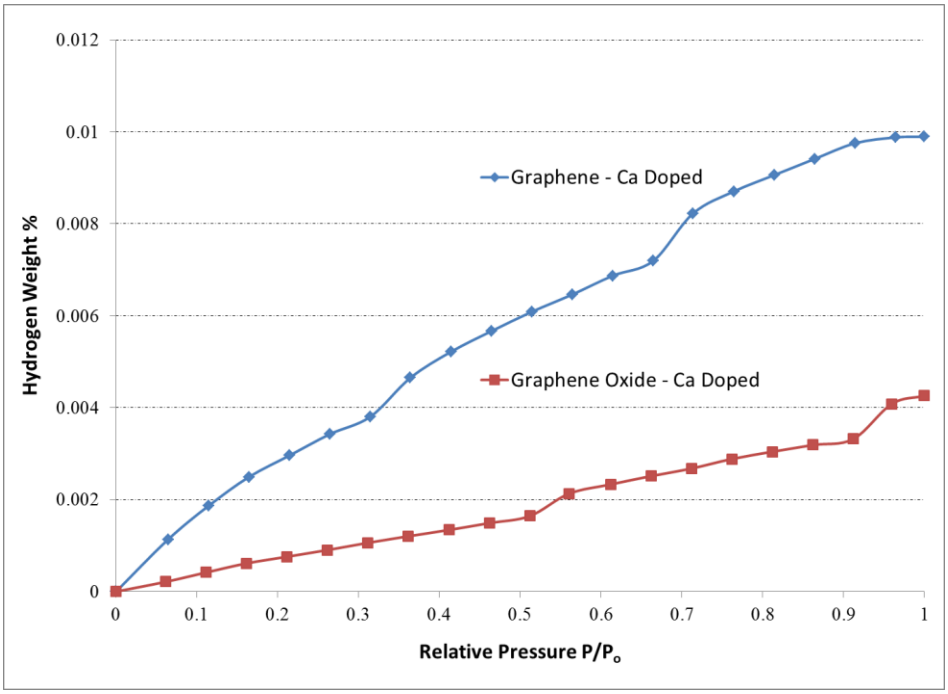

Figure 3.13 H_2 Storage at 77 K of G – Ca and GO – Ca

3.4.5. Heat of Adsorption Measurement

The isoteric heat of adsorption is a measure of the attraction of hydrogen to the surface and pores of the adsorbent. It is calculated using the Van't Hoff equation and utilizing adsorption isotherms at 77 and 87 K. When the heat of adsorption is in the range of 0 – 10 kJ/mol, hydrogen adsorption at liquid nitrogen temperature is favorable. Once the adsorption enthalpy approaches the range of 15 – 20 kJ/mol, room temperature (298 K) hydrogen adsorption is most favorable. Even though the calcium doped samples adsorbed a very small amount of hydrogen at 77 K, it may be due to their increased adsorption enthalpy which would result in a much higher storage at room temperature. Figure 3.14 shows the isoteric heats of adsorption of calcium doped grapheme at various

points of adsorption. The maximum adsorption enthalpy for this sample is about 0.62 kJ/mol.

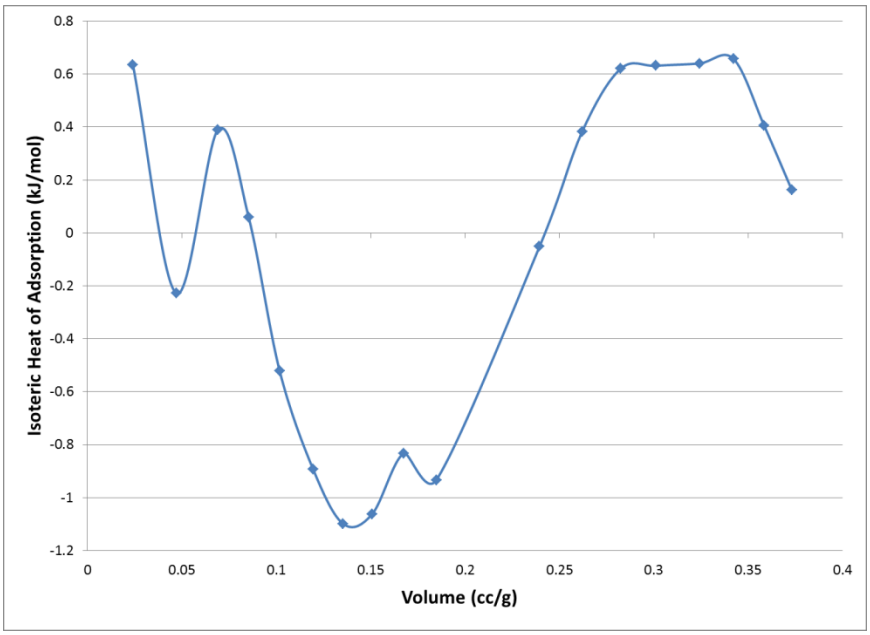

Figure 3.14 Heats of Adsorption for Calcium Doped Graphene

The range of adsorption enthalpies goes into the negative realm because the hydrogen storage of the material is extremely low which results in inconsistent results. The negative values show a repulsion of the hydrogen molecules with the surface of graphene. Figure 3.15 shows the heats of adsorption for calcium doped grapheme oxide. These results are much more consistent with literature due to its higher storage capacity at 77 and 87 K. The range of adsorption enthalpies are from 6 – 1 kJ/mol. This is better than the calcium doped graphene complex, yet still far away from the 15 – 20 kJ/mol range for hydrogen storage at room temperature.

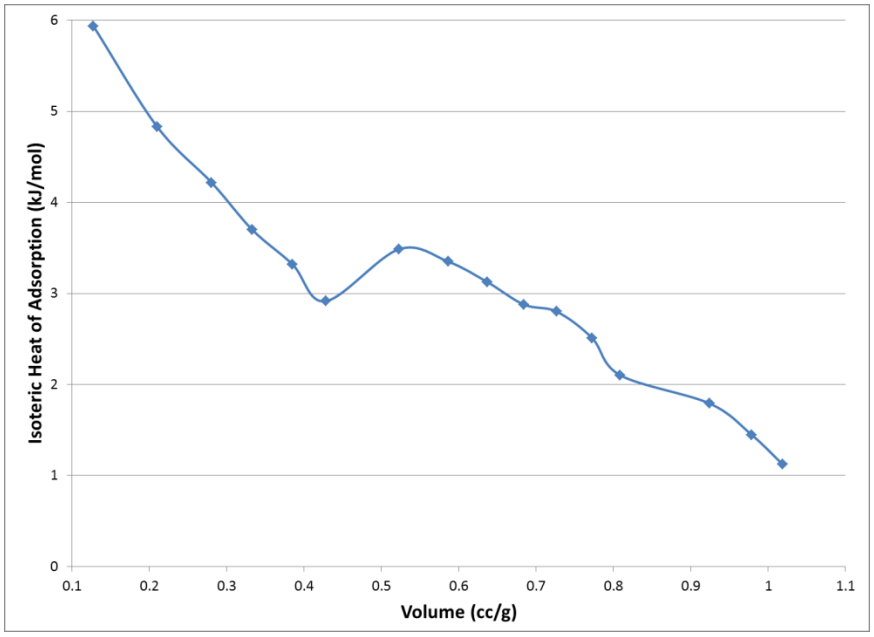

Figure 3.15 Heats of Adsorption for Calcium Doped Graphene Oxide

3.4.5. Calcium Doping of G and GO Summary

FT-IR results show a successful doping of calcium on the graphene and graphene oxide layers. The calcium atoms were proven to cluster and cause a decrease in surface area that resulted in a surface area that is highly unsuitable for hydrogen storage. The hydrogen storage measurement at 77 K demonstrated graphene's superiority over graphene oxide for hydrogen storage. The calcium doped graphene complex proved to have a hydrogen storage capacity of over 120% greater than its graphene oxide counterpart. However, the storage capacity of 0.01 weight % at 77 K is a relatively low storage capacity and, due to low adsorption enthalpies in the range of 1 – 6 kJ/mol, results in a negligible capacity at room temperature.

3.5. Exfoliation of Graphene and Graphene Oxide via Platinum

Exfoliation is the process of spacing graphene or GO sheets between other sheets while preventing face-to-face aggregation of the carbon sheets. This is vital in attaining and maintaining a high surface area material. Aggregation always occurs when removing G or GO from its dispersion and drying it. The theoretical surface area of graphene is calculated to be 2600 m^2/g. Any decrease in this area can be attributed to aggregation of the carbon sheets. It is estimated that around 60 graphene sheets agglomerate on top of each other into graphite-like bundles. Dried graphene shows a surface area of around 20 m^2/g, which is significantly less than 2600 m^2/g. Graphite stacks of carbon sheets are commonly defined as more than 10 sheets of carbon aggregated on top of each other. Aggregation lowers surface area and decreases accessible pores for gas adsorption [39].

Aggregation may be inhibited by impregnating the graphene sheets with spacers of either organic or metallic identity. Nanoparticles can be deposited on the graphene sheets when the graphene is in its dispersion form. These nanoparticles will act as structural supports for when the graphene is removed from the dispersion. Platinum (Pt) nanoparticles have been commonly used due to their size and reactivity with hydrogen. A chemical synthesis route of reduction of a metallic acid in the presence of a surfactant can deposit the metal nanoparticles on the carbon sheets [39]. Figure 3.16 shows the process of exfoliation using the platinum particles as spacers to prevent aggregation.

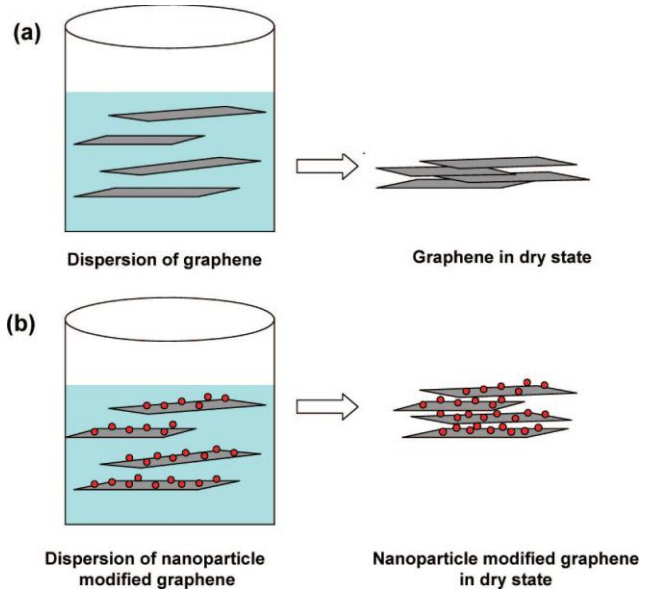

Figure 3.16 Exfoliation of Graphene Using Platinum Particles [39]

Platinum particles create spacing of a few nanometers between each carbon sheet, exposing more of the carbon sheets for gas adsorption. Both graphene and graphene oxide will be investigated to determine if platinum nanoparticles can increase the surface area by preventing agglomeration of carbon sheets.

3.5.1. Synthesis of G and GO Exfoliation via Pt Particles

All starting materials are purchased from Sigma Aldrich unless specified differently. The graphene used is reduced graphene oxide (rGO) made from the reducing agent DMH as reported in section 3.2.3. The synthesis is identical for graphene and graphene oxide, besides when taking into account weight ratios of Pt to G or GO. The chemical reduction of Chloroplatinic acid in the presence of the surfactant 3-(N,N-dimethyldodecylammonio) propanesulfonate (SB12). First, water soluble graphene or graphene oxide is developed in order to ensure G or GO is dispersed in DI water.

Graphene was synthesized using the route for reduction found in 3.3.3 Synthesis Route via N,N-Dimethylhydrazine. GO was synthesized using the modified Hummer's method also discussed in the same section. 20 mg of G/GO is dispersed in 50 mL of DI water and then ultrasonicated for 30 minutes. Aqueous solutions were left overnight to ensure dispersions were sufficiently synthesized. Then 60 mg of Chloroplatinic acid hexahydrate is dissolved in 10 mL of DI water. This solution is adjusted to a pH of about 7 with the use of sodium carbonate. This solution is then added to the G/GO aqueous solution. 39 mg of the surfactant 3-(N,N-dimethyldodecylammonio) propanesulfonate (SB12) is added into 15 mL of methanol and then added into the G/GO solution. This solution is then adjusted to a pH of 7 via sodium carbonate. This reaction solution is then kept at 80 °C for 90 minutes. After the time has passed, about 10 mL of 1M Hydrochloric acid is added into the solution in order to precipitate the Pt-G/GO solid from the solution [39]. The product is removed via vacuum filtration with rinsing of methanol and DI water to remove unreacted particles. The filter used is a Whatman qualitative grade 2 (8 μm) filter paper. The filtrate should be clear to indicate complete reduction occurred. This synthesis is 50 weight % of platinum to carbon ratio. Ratios of 1, 10, and 50 weight % of platinum to carbon atoms were synthesized for GO exfoliation in order to determine the optimum ratio.

3.5.2. FT-IR Characterization of Pt-Graphene/Graphene Oxide

Fourier Transform Infrared spectroscopy is used to confirm no side reactions occurred during the reaction. The platinum particles are being deposited on the surface of the carbon sheets, yet there are no chemical reactions occurring during process. It should

also be noted that FT-IR shows organic bonds and platinum particles will not show up in the spectrum. The FT-IR spectrum should confirm that no new functional groups are present in both of the compounds. Figure 3.17 compares the FT-IR of rGO and rGO – Pt exfoliated.

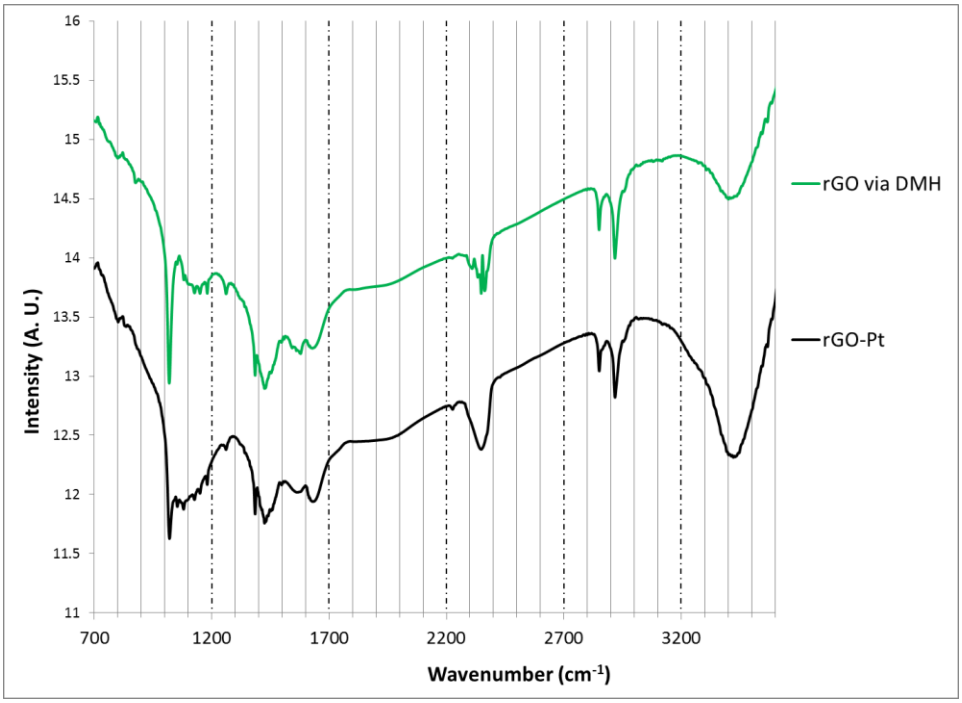

Figure 3.17 FT-IR of rGO (untreated) and rGO-Pt Exfoliated

As you can see in Figure 3.17, the spectrum of rGO (untreated) and rGO – Pt exfoliated are nearly identical, which confirms no undesired side reactions or impurities entered the reaction during the exfoliation process. Figure 3.18 compares graphene oxide (untreated) to GO – Pt exfoliated. It appears most of the peaks are identical. However, a conjugated peak at 2850 cm^{-1} and 2910 cm^{-1} appears in the GO – Pt product. These peaks can be attributed to the C-H and C-CH_3 bonds that are present in both compounds, yet appear more distinct in the exfoliated product.

Figure 3.18 FT-IR of GO (untreated) and GO – Pt Exfoliated

3.5.3. X-Ray Diffraction Characterization

X-ray diffraction (XRD) was performed on a sample of graphene oxide – platinum. The main purposes of XRD of this sample were to confirm the complete reduction of the Chloroplatinic acid and to calculate the crystallite size of the platinum particles. Figure 3.19 shows the XRD pattern of GO-Pt (1 wt. %) and GO control (untreated) sample.

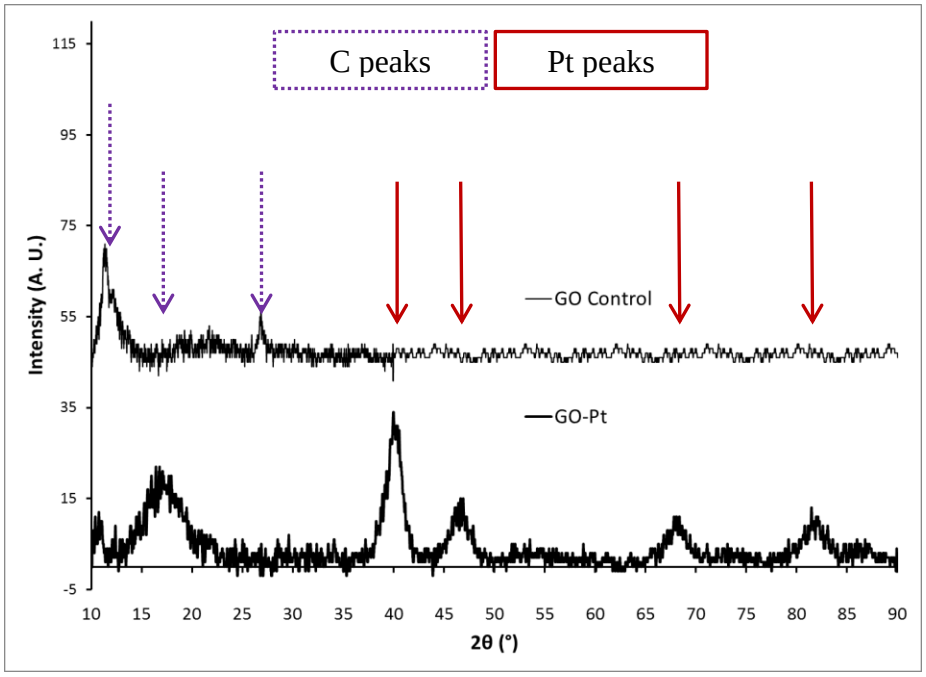

Figure 3.19 XRD Pattern of GO and GO-Pt (1 wt.%)

The figure above shows a legend that tells one which peaks are attributed to carbon and platinum appearing in the crystal lattice. It is very clear that the platinum did deposit into the sheets of graphene oxide. The platinum peaks are the common face-centered cubic lattice (fcc) crystal lattice formation that usually characterizes platinum particles. The peaks for Pt are: 40°, 46°, 67°, and 83°. The decrease in intensity of the carbon peak at 26° is indicative of reduced aggregation. This peak arises in graphite because of the aggregation of carbon sheets. This peak disappears for the platinum exfoliated graphene oxide which proves an increase in surface area should be expected.

It is necessary to also calculate the particle size of the platinum nanoparticles on the carbon sheets. The crystallite size was determined using the Scherrer formula, equation 2.2, which has been re-stated below. By analyzing the Pt peak at 40°, the crystallite size of the tetrahedral-shaped Pt particles was determined to be in the range of

6.9-9.7 nanometers. It has been determined that an ideal size of 1-3 nanometers is optimum for maximum exfoliation of the carbon sheets [39].

$$\tau = \frac{K\lambda}{\beta \cos \vartheta} \tag{3.1}$$

3.5.4. Surface Area Characterization

Surface area tests were performed on all samples because this is the attribute that is being optimized with platinum exfoliation. Nitrogen adsorption of every sample from the relative pressure range of 0.05 to 0.3 was used with equation 2.3, in order to determine the BET specific surface area of each sample. Mass ratios of 1, 10, and 50 weight % of platinum to carbon ratios were synthesized and test. Figure 3.20 shows the nitrogen adsorption plots of 1, 10, and 50 weight % of platinum to carbon of graphene oxide – platinum and reduced graphene oxide – platinum samples.

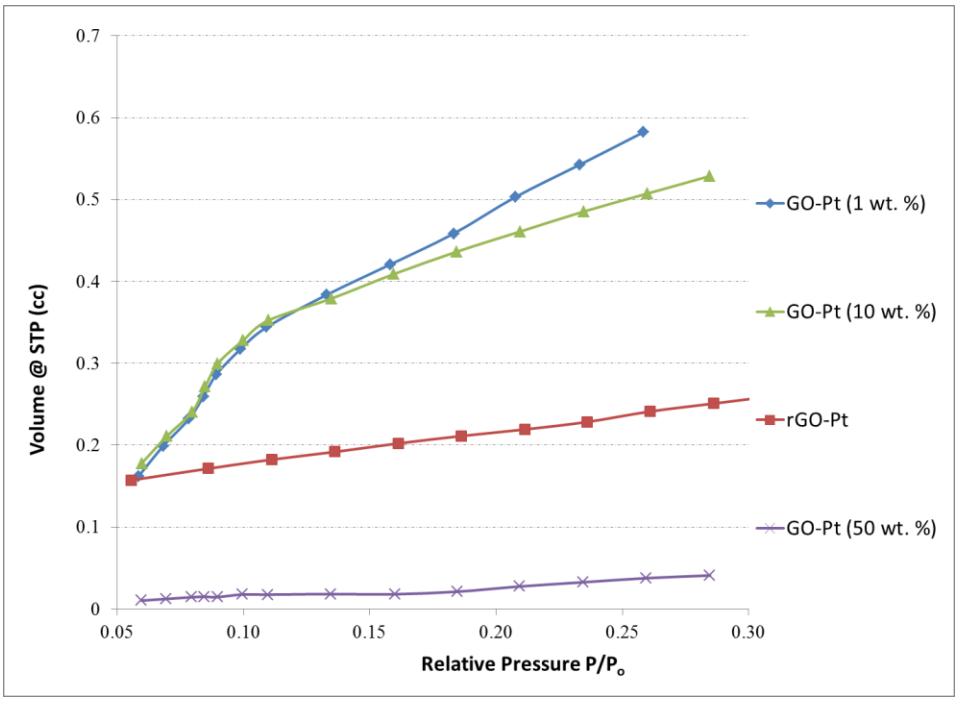

Figure 3.20 BET N_2 Adsorption Plot of GO-Pt and rGO-Pt Samples

The surface area of the samples and the graphene oxide control, or untreated, sample are shown in Table 3.4. Table 3.5 compares the reduced graphene oxide – platinum sample with the control reduced graphene oxide and untreated graphene that was purchased from Angstrom Materials. This reduced graphene oxide was synthesized by using L-ascorbic acid as the reducing agent.

Table 3.4 BET SSA of GO-Pt Samples

Sample Name	BET SSA (m^2/g)
50 Weight %	1.7
10 Weight %	50.1
1 Weight %	65.2
GO Control	18.8

Table 3.5 BET SSA of rGO-Pt and Control Samples

Sample Name	BET SSA (m^2/g)
rGO – Pt	11.4
rGO Control	2.6
Graphene (untreated)	11.3

By analyzing Table 3.4, it appears that the optimum surface area is around the 1 weight % ratio of platinum to carbon atoms. At higher ratios of 10 or 50 weight %, the platinum particles seem to actually cause a lowering of surface area probably due to their clustering on the surface of the substrate. It is a challenge to evenly disperse the platinum particles across the carbon sheets to minimize clustering and a decrease in surface area. Table 3.5 shows the unaltered change that the platinum particles had on the reduced graphene oxide complex. It appears that either clustering of the platinum particles or misplacement of the particles led to a low surface area material of only 11 m^2/g.

3.5.5. Hydrogen Sorption Measurements at 77 K

Hydrogen adsorption was measured for both rGO – Pt exfoliated and GO – Pt exfoliated and compared to each other and their respective untreated form. The storage capacity at 77 K should increase since platinum is increasing the surface area of the material. Platinum is also causing a spillover effect to occur by disassociating the hydrogen molecules into atoms that are more susceptible to adsorb onto the surface and in the pores of the material. Figure 3.21 shows the adsorption of hydrogen of the exfoliated samples in comparison with untreated graphene oxide.

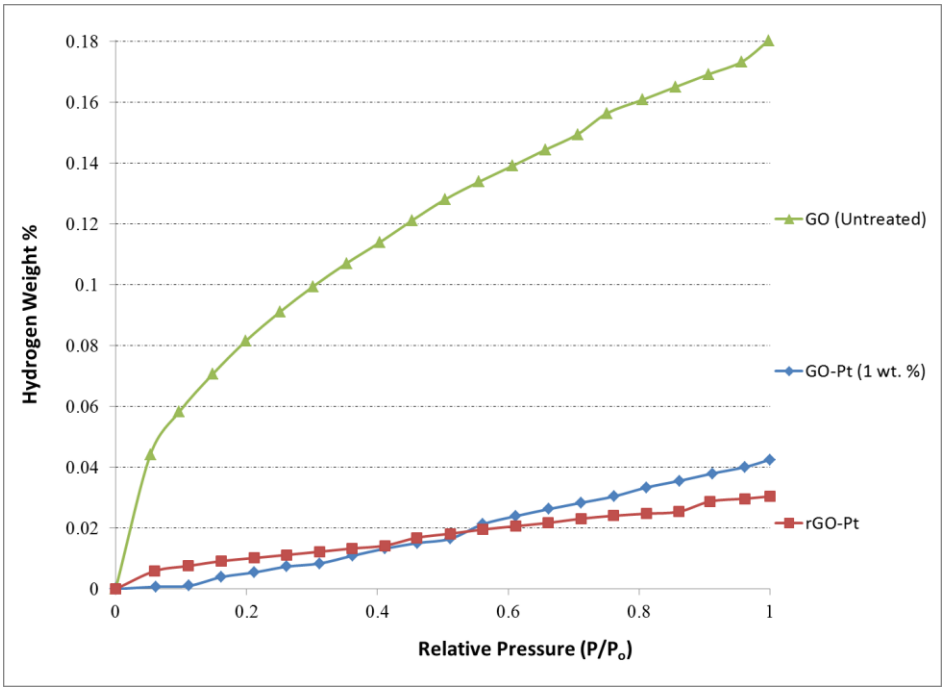

Figure 3.21 H_2 Storage at 77 K of GO-Pt, rGO-Pt, and GO

It appears that the maximum storage at 77 K and up to 1 atmosphere of pressure is 0.045 weight % and 0.025 weight % for GO – Pt (1 wt. %) and rGO – Pt, respectively. Graphene oxide and exfoliated graphene oxide appear to have nearly identical saturation

levels of hydrogen adsorption. The storage capacity of GO – Pt is higher than rGO – Pt because of the diminished surface area of the rGO – Pt sample. However, the storage capacity of graphene oxide (untreated) still remains higher than both platinum exfoliated complexes.

3.5.6. Platinum Exfoliation Summary

Exfoliation via platinum particles has the sole purpose of reducing aggregation of the carbon sheets and maintaining a high surface area material suitable for hydrogen storage. FT-IR characterization proved that no unwanted reactions occurred during the synthesis. XRD also proved that the platinum was succesfully reduced into the carbon material. The particle size of platinum was calculated to be in the range of 7 – 10 nanometers, which is much larger than the desired 1 – 3 nanometer range. This problem causes a decrease in surface area and exposure sites for adsorption of hydrogen. BET surface area results show that the 1 weight % of platinum to carbon ratio is ideal for the most optimum surface area. Hydrogen storage is optimum for this ratio with the GO – Pt sample in which the sample stores up to 0.045 weight %. However, this storage capacity is lower than untreated graphene oxide, which means there is no measurable change in exfoliating the GO or rGO samples with platinum particles.

3.6 Cross-Linking of GO via Organic Spacers

Not only can cross-linking (CL) be performed by metallic particles; organic spacers may also be used. The ideal situation is to decrease aggregation of the carbon sheets with taking up as minimal space as possible between the sheets. Graphene oxide

has an inherit spacing of 0.7 nanometers. The majority of this space is filled by hydroxyl and carboxyl groups, which also inhibit hydrogen adsorption. Utilization of the oxygen functional groups to increase the interlayer spacing, without filling the space between the sheets, is the target of this modification technique.

The reactivity of oxygen can be taken advantage of here to connect the carbon sheets with an organic spacer. The well-established reactivity of oxygen and Boronic acid is utilized here to cross-link the graphene oxide sheets to form a graphene oxide framework (GOF) [34]. The linker selected controls the pore shape and volume of the graphene oxide framework. Boronic acid has been shown to optimize the surface area and is of a relatively small molecular size since boron has an atomic number of 3 in the periodic table [34]. Grand Monte Carlo simulations (GMCs) demonstrate the potential of a graphene oxide framework adsorbing up to 10 weight % of hydrogen [34]. Figure 3.22 shows the GMCs of various GOFs of different linker per carbon ratios at 77 K. For instance, GOF-32 refers to a graphene oxide framework synthesized with 1 Boronic acid linker per carbon atom.

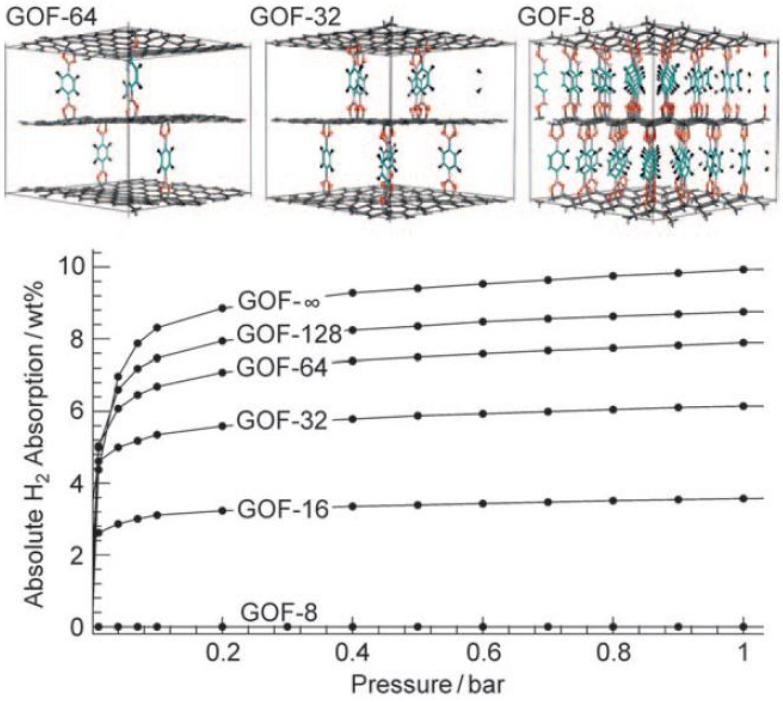

Figure 3.22 Grand Monte Carlo Simulation of Various GOFs [34]

As Figure 3.22 shows, GOFs at higher linker to carbon ratios are more optimized for hydrogen adsorption due to the maximum unoccuppied space in the framework since very few linkers are present. This does lead to higher pore volume and gas adsorption; however, the instability of the framework is at risk and more linkers need to be added for structural support. An optimization was calculated to determine that 1 linker per 32 carbon atoms upholds structural stability and still has accesible pores for gas adsorption [34]. Density functional theory lattice dynamics calculations prove structural stability and GMCs show hydrogen storage of about 6 weight % at 77 K and 1 bar. The cross-linker being used is 1,4-benzene diboronic acid (B14DBA), which has a special affinity for the hydroxyl groups on the graphene oxide surface. Figure 3.23 shows the strcutural configuration of B14DBA. Note the functional groups of the phenyl ring and boron ester groups.

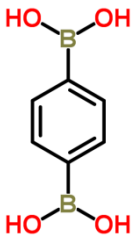

Figure 3.23 Chemical Structure Diagram of B14DBA

Figure 3.24 shows the reaction occurring with B14DBA and the –OH groups of the graphene oxide sheets.

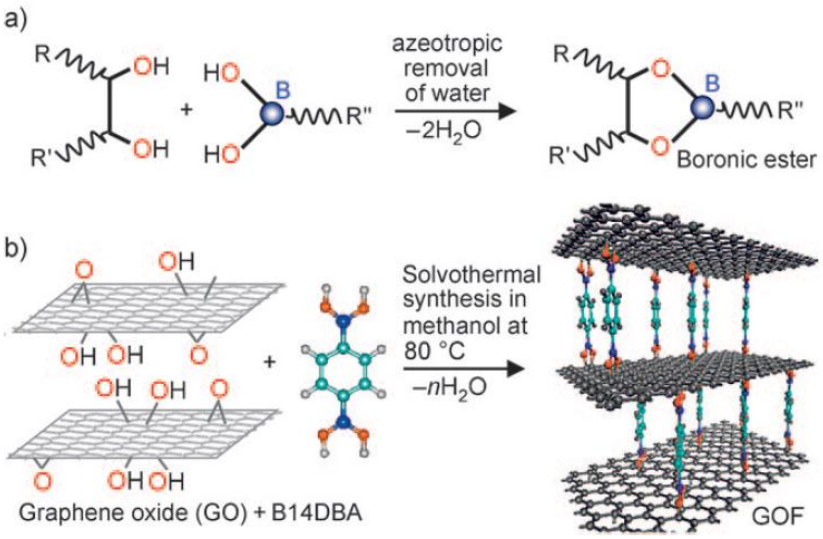

Figure 3.24 (a) Boronic Ester Formation (b) GOF Formation with B14DBA [34]

The framework is complete when the ester connects on both sides to the carbon sheets as seen at the end of part (b) of Figure 3.24. The reaction process used is a solvothermal synthesis. This synthesis consists of placing a precursor solution in an autoclave (high-pressurized container) for an extended amount of time at a specific temperature. The particle size and distribution can be controlled by the solvent and

reaction temperature. Various solvents will be investigated for their cross-linking capabilities and surface area effect on the product.

3.6.1. Solvothermal Synthesis Route for GOFs

All starting materials were purchased from Sigma Aldrich unless otherwise specified. Dispersions of graphene oxide in various solvents need to be synthesized before the reaction can begin. Every dispersion was ultrasonicated using the QSonica Q500 for 30 minutes and left overnight to ensure a dispersion was synthesized. The most promising weight ratio was a 1:1 of GO to B14DBA; therefore, 1 gram of 1,4-benzene Diboronic acid is added for every 1 gram of GO used in the dispersion. For a typical synthesis, 200 mg of graphene oxide (synthesized via modified Hummer's method) is dissolved in 20 mL of the given solvent, which consist of Ethanol, Methanol, Tetrahydrofuran (THF), and N-Methyl-2-pyrrolidone (NMP). The dispersion was then ultrasonicated for 30 minutes and then 200 mg of 1,4-benzene Diboronic acid (B14DBA) is stirred into the mixture. The mixture was vigorously stirred until all of the B14DBA was dissolved. At times, bath sonication using the MTI Sonicator was required to assist stirring. The solution was then placed in the 55 mL stainless steel autoclave developed by Emre Demirocak. The autoclave was sealed air-tight and placed in a dry oven at 80 °C for 72 hours. The autoclave was shaken every 5 or so hours to keep the settling GO in the dispersion. The autoclave is then removed from the oven and left to cool to room temperature. The solution is then centrifuged at 5000 rpm for 30 minutes. The solution is decanted and then further filtrated through vacuum filtration. The filter used is a Whatman qualitative grade 2 (8 μm) filter paper. The product is then repeatedly washed

with the corresponding solvent used in the synthesis to remove unreacted GO particles. The solution is then washed with water and outgassed in an oil bath at 80 °C for 24 hours.

3.6.2. FT-IR Characterization of GO Cross-Linked Samples

FT-IR was an important characterization technique for the cross-linking synthesis because it proved whether the Boronic acid spacers correctly reacted within the carbon sheets to form the GOF. FT-IR can directly tell one if the correct bonds were formed and to what extent cross-linking is present throughout the graphene oxide framework. The primary bond is the B-O bond that attaches with the hydroxyl groups of the carbon sheets. FT-IR can also distinguish whether an impurity phase is present or not in the product due to the cross-linker reacting with other groups on the carbon sheets. Figure 3.25 shows the FT-IR of GO cross-linked in various solvents, GO control sample, and 1,4-benzene Diboronic acid (B14DBA).

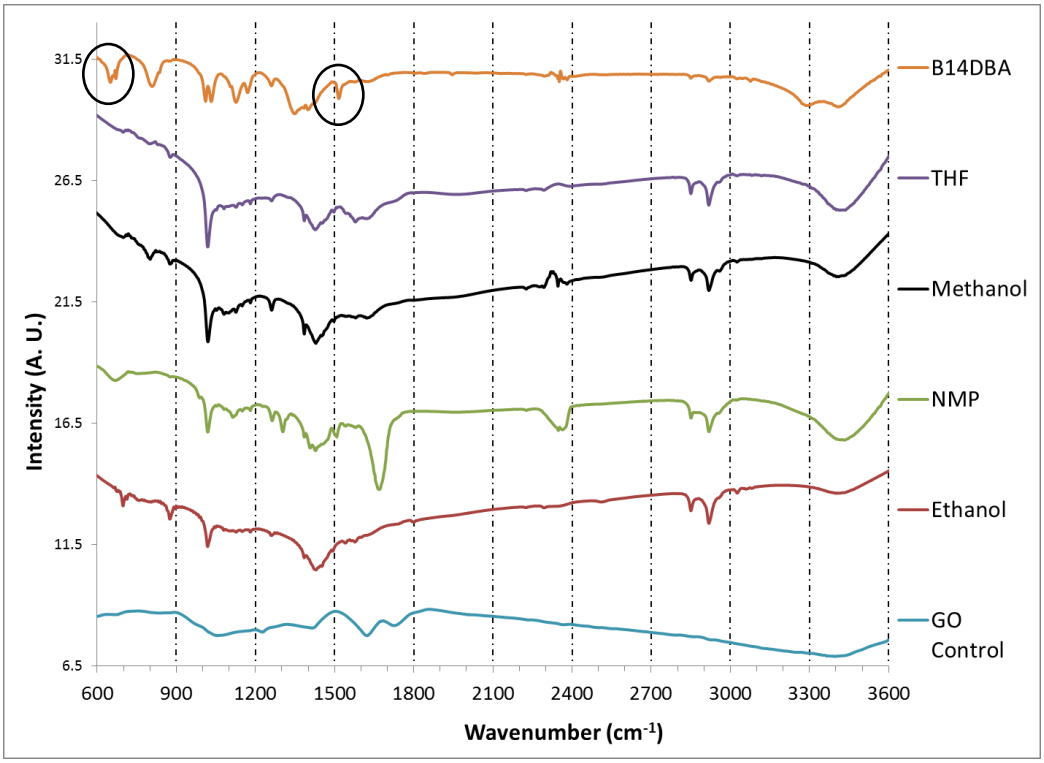

Figure 3.25 FT-IR Plot of GO Cross-linked in Various Solvents

Figure 3.25 shows the spectrum of graphene oxide after being cross-linked in the solvents of methanol, ethanol, THF, and NMP. The spectrum of the cross-linker B14DBA and a control sample of graphene oxide are also shown for comparison. Important signals of B14DBA are the B-O deformation peak at 675 cm^{-1} and the phenyl ring carbon double bond signal at 1522 cm^{-1}. Both of these signals are circled on the B14DBA spectrum. The B-O peak is seen in the methanol, ethanol, and NMP products, in which shows the sharpest peak in the ethanol solvent. The carbon double bond phenyl peak is only very slightly present in the ethanol product. An absorbance band in between 1250 cm^{-1} and 1400 cm^{-1} corresponds to the B-O groups connected with the various functional groups of the graphene oxide sheets. This absorbance band slightly appears in all of the samples, but most prominent in the NMP product. NMP and ethanol are the best

candidates for the cross-linking synthesis. However, NMP appears to have an impurity phase from the B14DBA at 1100 cm^{-1}. With this being taken into account, ethanol appears to be the best solvent for the solvothermal synthesis to cross-link graphene oxide.

3.6.3. Surface Area Characterization of Cross-Linked Samples

Surface area is the primary motivation for this modification technique of graphene oxide. Surface area measurements were performed using BET theory nitrogen adsorption isotherms at 77 K. 11 point BET theory utilizes the nitrogen adsorption curves from the relative pressure range of 0.05 to 0.3, while taking 11 data points within said pressure range. Figure 3.26 shows the adsorption isotherms for the various GOFs in their solvents.

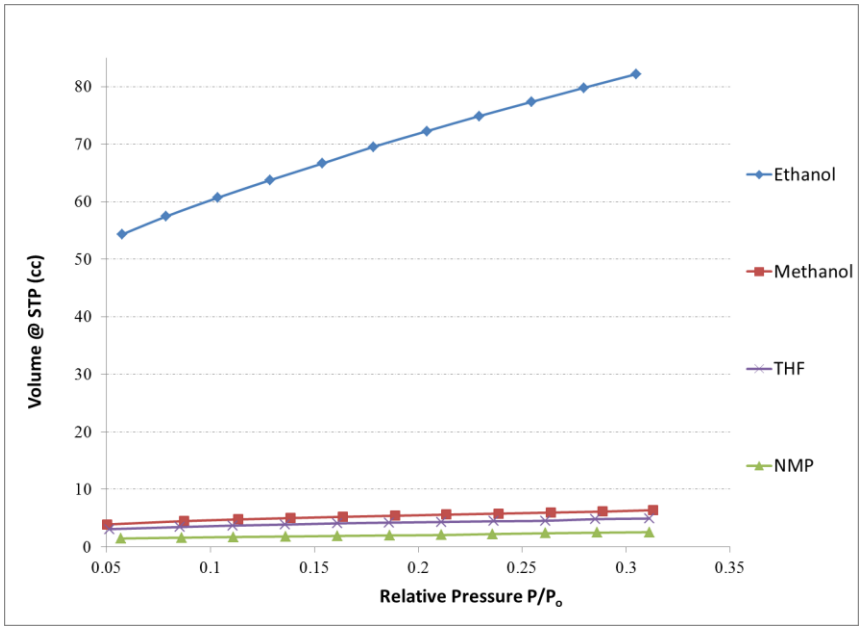

Figure 3.26 N_2 Adsorption Isotherms of Cross-Linked GO Samples at 77 K

It appears from Figure 3.26 that the GO product from the ethanol solvothermal reaction has the highest adsorption of nitrogen at 77 K. The respective BET specific surface areas are shown in Table 3.6.

Table 3.6 BET SSA of GO CL in Various Solvents

Sample Name	BET SSA (m2/g)
Ethanol	324.2
Methanol	19.5
NMP	8.1
THF	15.2
GO Control	18.8

The highest surface area was the graphene oxide cross-linked in ethanol product, with a surface area of 324 m^2/g. The other products only had surface areas in the vicinity of the graphene oxide control. It appears that the cross-linking reactions with the graphene oxide sheets only occurred in this product. Partial reactions occurred with low instability causing the carbon sheets to aggregate and decreasing the surface area.

3.6.4. Hydrogen Sorption Measurements at 77 K

The hydrogen capacity was measured on every cross-linked sample, even though it is unnecessary for the low surface area samples. This is because at 77 K, the only factor for hydrogen storage is surface area and any area below 100 m^2/g is considered too small for sufficient gas adsorption. Figure 3.27 shows the hydrogen adsorption isotherm of graphene oxide with the various solvents along with the control sample of graphene oxide.

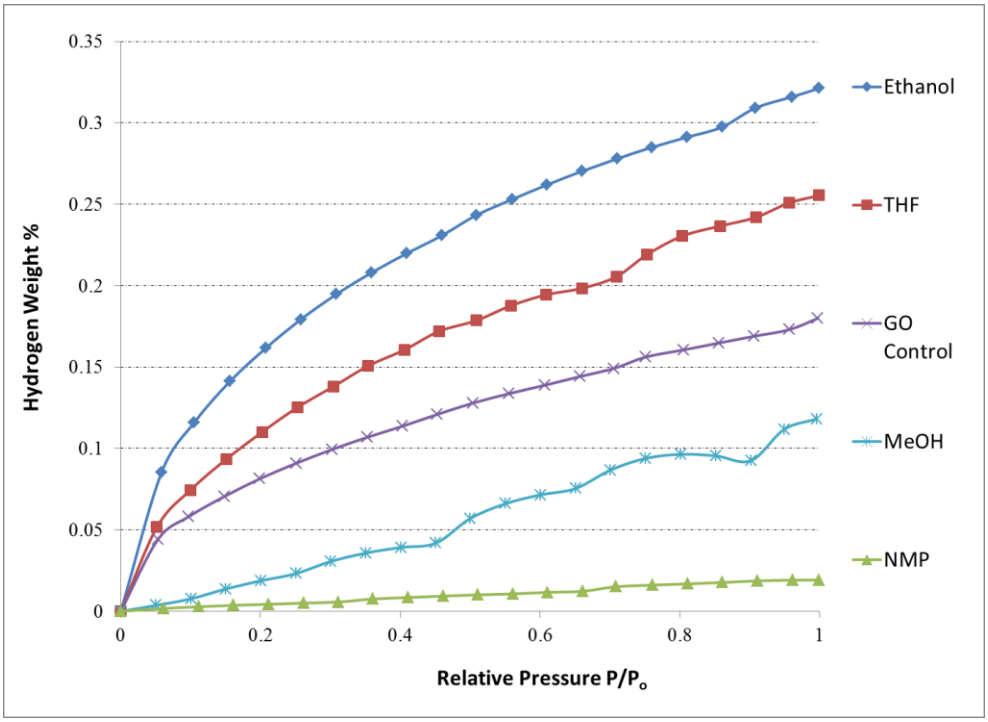

Figure 3.27 H_2 Adsorption of Cross-Linked GO at 77 K

The maximum hydrogen storage at 77 K was performed by the cross-linked sample in ethanol at a storage capacity of 0.33 weight %. GO cross-linked in THF had a close capacity of 0.26 weight %. Both of these capacities were increased from the untreated graphene oxide sample with a storage capacity of 0.18 weight %. The graphene oxide cross-linked in NMP product experienced a decrease in storage capacity due to its dramatic decrease in its surface area (8.1 m^2/g). This same phenomenon occurred with the cross-linked sample in Methanol, storage capacity decreased from 0.18 m^2/g to 0.12 m^2/g. The surface area of the Methanol cross-linked sample remained about constant with the control; therefore, it appears the organic spacers are impeding hydrogen access to the pores of graphene oxide.

3.6.5. Cross-Linking of Graphene Oxide Summary

Cross-linking of graphene oxide had the sole purpose of increasing the interlayer spacing between the carbon sheets in hopes of increasing hydrogen adsorption. FT-IR shows that the cross-linker, 1,4-benzene Diboronic acid, was successfully incorporated into the graphene oxide network of the cross-linked GO in ethanol and NMP samples. BET surface area measurements showed that ethanol was the only solvent to dramatically increase the surface area of graphene oxide to 324 m^2/g. Hydrogen adsorption measurements complemented the BET results showing the GO CL with ethanol had the highest hydrogen uptake of 0.33 weight %. This was a 70% increase from the untreated graphene oxide sample. GO CL in THF also showed a 45% increase from the untreated graphene oxide. These results show an improvement in the surface area and gas adsorption at 77 K through the cross-linking modification technique.

3.7. Polyaniline-Based Composites

Polyaniline (Pani) is one of the most researched polymers because of its conducting and electronic properties. It is considered to be a conducting polymer with a salt and base form of different properties. The synthesis of Pani is a facile route that also attracted researchers in the fields of energy storage, light-emitting diodes, sensors, catalysis, and capacitors [40]. The emeraldine base form of Pani will be investigated in this thesis to incorporate into a composite with graphene and graphene oxide. The emeraldine base form's chemical structure is shown in Figure 3.28. The base form of Pani contains benzenoid and quinoid rings that give a unique functionality to the complex. Polyaniline utilizes its surface area in order to take part in physisorption of

hydrogen molecules. This aspect is the main concern of this part of the research. Pani and other polymers have been the focus of controversial publications in the past [41]. Many groups reported storage capacities of 6 – 8 weight % at room temperature, but were later refuted by other groups that could not reproduce their results [42]. Polyaniline will be utilized as a substrate for embedding graphene and graphene oxide sheets into the complex. Storage properties at room temperature and surface area will be investigated to determine an optimum complex with various forms of graphene and graphene oxide.

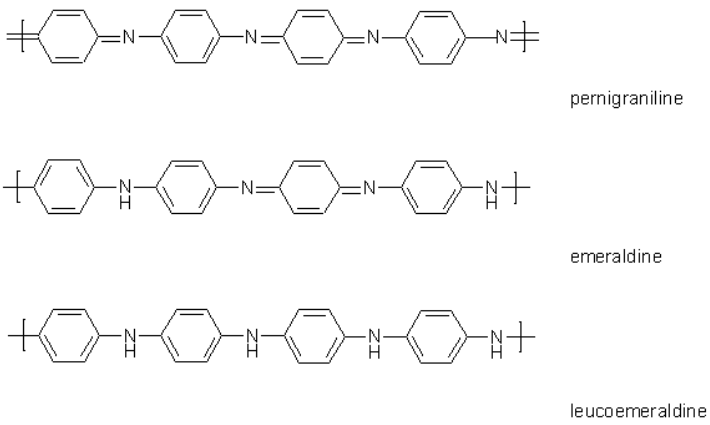

Figure 3.28 Various Forms of Polyaniline [42]

3.7.1. Synthesis of Bulk Polyaniline

This is the synthesis route to develop the emeraldine base of Pani in its natural fiber form without any surface morphology modification. The route to synthesize Pani was an oxidative polymerization method of the "rapid mixing" technique. The oxidant of choice is ammonium persulfate (APS) and the doping acid used was hydrochloric acid. For a typical synthesis, 9.5 mL of aniline is stirred with 200 mL of 1M HCl in a flask. Another flask is prepared by mixing 2.28 grams of APS with 200 mL of HCl. Both solutions are stirred for 20 minutes to ensure complete mixing. The APS solution is then

rapidly poured into the aniline solution and left to stir for 24 hours at room temperature. Vacuum filtration was then performed using a 11 μm pore size filter. Solution was rinsed with 1M HCl to remove unreacted aniline. Product was then dried under vacuum in an oil bath at 80 °C for 24 hours.

3.7.2. Synthesis of Pani-Graphene and Pani-Graphene Oxide

The composites of Pani with graphene and graphene oxide were synthesized by an identical method from section 3.7.1. The graphene, graphene oxide, or any other modified G/GO complex was added to the 9.5 mL of aniline and 200 mL of HCl before the polymerization reaction began. The amount of graphene or graphene oxide varied from 1:0.05 to 1:0.1 molar ratio of moles of aniline to moles of graphene/graphene oxide. The entirety of the synthesis remains the same besides this addition step of the G/GO.

3.7.3. FT-IR Characterization of Pani, Pani-G, and Pani-GO

FT-IR spectroscopy was utilized to determine successful polymerization and formation of the polymer composite. It is important that no unexpected bonds are formed between Pani and graphene or graphene oxide. The composite is a physical composite, there are no chemical reactions occurring between Pani and the G/GO compound. Figure 3.29 compares the spectra of graphene oxide, Pani, and Pani-graphene oxide to determine successful polymerization. The distinct peaks of Pani are the benzenoid and quinoid ring signals at 1450 and 1560 cm^{-1}, respectively. Both of these peaks are prominent in the Pani-graphene oxide spectrum. The peak at 1300 cm^{-1} in the Pani and Pani-graphene oxide spectra represent the π-electron localization due to the protonation of Pani. There is

a very sharp peak at 1375 cm^{-1} that is due to the C-N bonds throughout the Pani complex. This peak is also found in the Pani-graphene oxide complex. The FT-IR shows successful polymerization of aniline and addition of graphene oxide to the Pani complex.

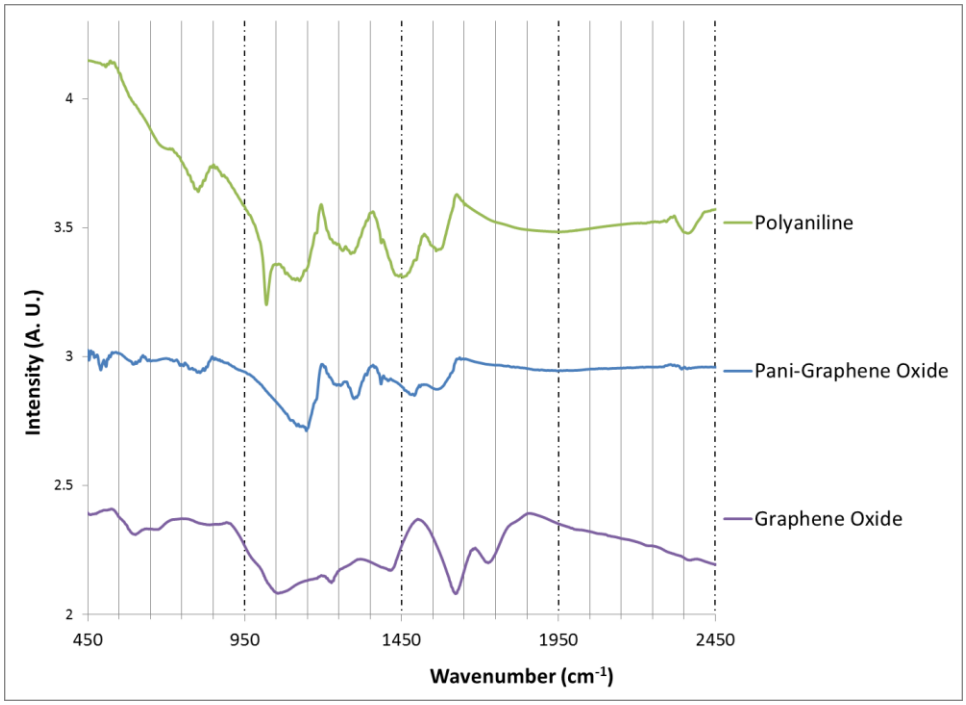

Figure 3.29 FT-IR of Pani, Pani-Graphene Oxide, and Graphene Oxide

Figure 3.30 shows the FT-IR spectra of Pani, graphene, and Pani-graphene in order to compare and determine successful formation of the composite. The benzenoid and quinoid ring signals at 1450 and 1560 cm^{-1}, respectively, are both found in the Pani-graphene composite. The signal around 1300 cm^{-1} for the π-electron localization of Pani is also present in the Pani-graphene complex. The C-N peak at 1375 cm^{-1} is also found in the Pani-graphene spectrum as a very distinct peak. According to FT-IR, it appears that the aniline was successfully polymerized while the graphene was an additive in the complex to form the Pani-graphene composite.

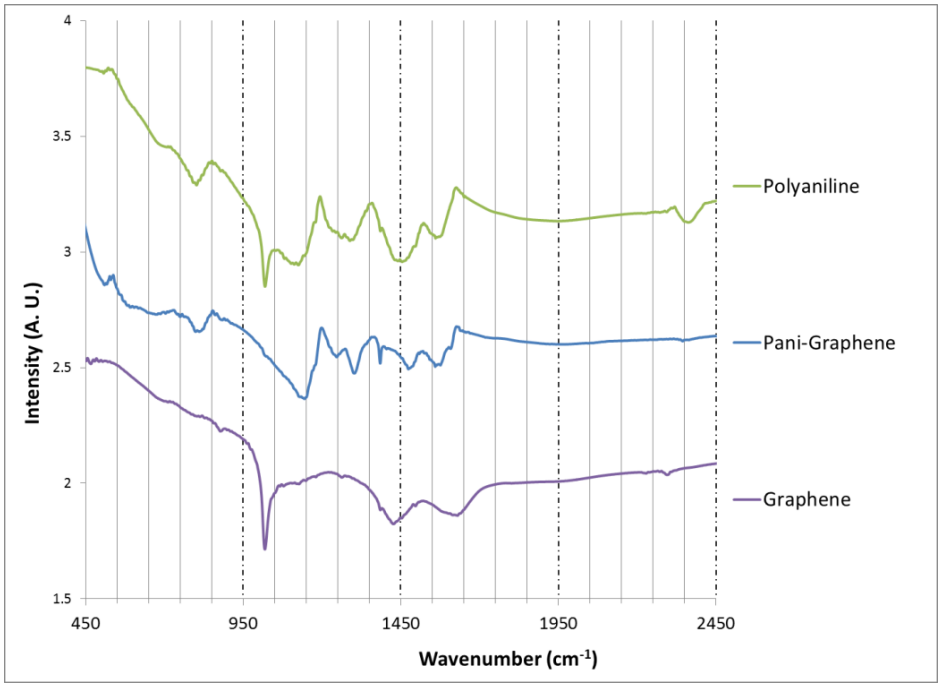

Figure 3.30 FT-IR of Pani, Graphene, and Pani-Graphene

3.7.4. Thermal Gravimetric Analysis of Pani-G and Pani-GO

Thermal gravimetric analysis (TGA) was performed on the Polyaniline – graphene and Polyaniline – graphene oxide samples in order to determine the thermal stability of the compounds at elevated temperatures. This is critical when determining if synthesis and outgassing procedures will compromise the stability of the complex. Figure 3.31 shows the thermal stability plot of both polymeric complexes. The first drop in weight loss should be noted as water vapor loss as the temperature approaches 100 °C. The stability of both compounds appears to be in the range of 110 °C – 175 °C.

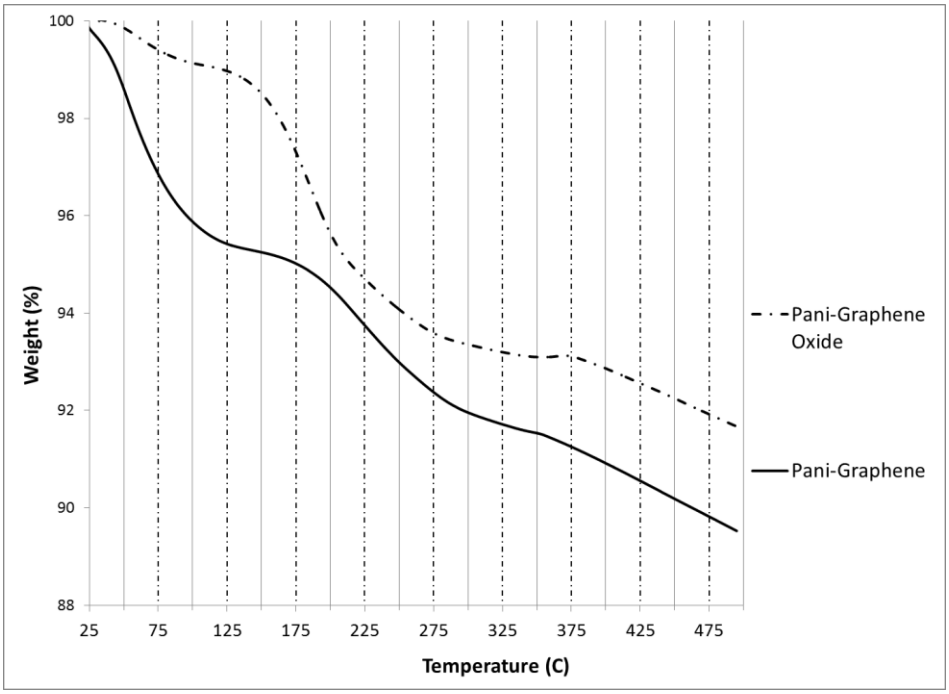

Figure 3.31 TGA Plot of Pani-G and Pani-GO

3.7.5. Surface Area Characterization of Pani-G and Pani-GO

Surface area measurements were run for the various molar ratios of Pani-graphene in order to determine an optimum ratio of Pani to graphene.. The primary purpose of these test are to show if a critical reduction in surface area occurred when adding the graphene to the polymer matrix. Table 3.7 shows the surface areas of the various ratios of Pani-graphene products. The ratio refers to mols of aniline: mols of graphene in the composite. It appears that the ratio of 1:0.05 and 1:0.1 maintain a surface area around 35 m^2/g. With taking into the error of Autosorb1, the values of 35.9 and 36.6 m^2/g are negligibly the same value. The molar ratio of 1:1 reduced the surface area of Pani from 24 to 10.3 m^2/g. Further measurements will be taken to determine which molar ratio of 1:0.1 or 1:0.05 is more ideal for hydrogen physisorption.

Table 3.7 BET Surface Area of Pani-G at Various Ratios

Sample Name	BET SSA (m2/g)
Polyaniline	24 [41]
Graphene	2.6
Pani-G (1:1)	10.3
Pani-G (1:0.1)	35.9
Pani-G (1:0.05)	36.6

Taking into effect the results from Table 3.7, the molar ratio of 1:0.05 of mols of aniline to mols of graphene will be considered the most optimum ratio. This ratio will be utilized in the polymeric complex with graphene oxide. The surface area was measured by BET theory to determine the degree of surface area loss from synthesis of the composite. Table 3.8 shows that the surface area increased to 31.1 m^2/g in the Pani-GO composite.

Table 3.8 BET Surface Area of Pani-GO and Controls

Sample Name	BET SSA (m2/g)
Polyaniline	24 [41]
Graphene Oxide	18.8
Pani-GO (1:0.05)	31.1

3.7.6. Hydrogen Sorption at 77 K of Pani-G and Pani-GO

Hydrogen storage at liquid nitrogen (77 K) temperature was measured for the polymer composites using Autosorb 1 made by Quantachrome Instruments. This adsorption measurement is at a low pressure; pressure range for adsorption is from 0 to 1 atm. Figure 3.32 shows the hydrogen storage of Pani-G and Pani-GO at 77 K. Both composites are synthesized using the 1:0.05 molar ratio of aniline to G/GO. The storage capacity was measured to be 0.019 wt. % and 0.016 wt. % for Pani-G and Pani-GO, respectively. The slight increase in hydrogen storage might be due to the Pani-G composite's larger surface area of 36.6 m^2/g compared to 31.1 m^2/g for Pani-GO.

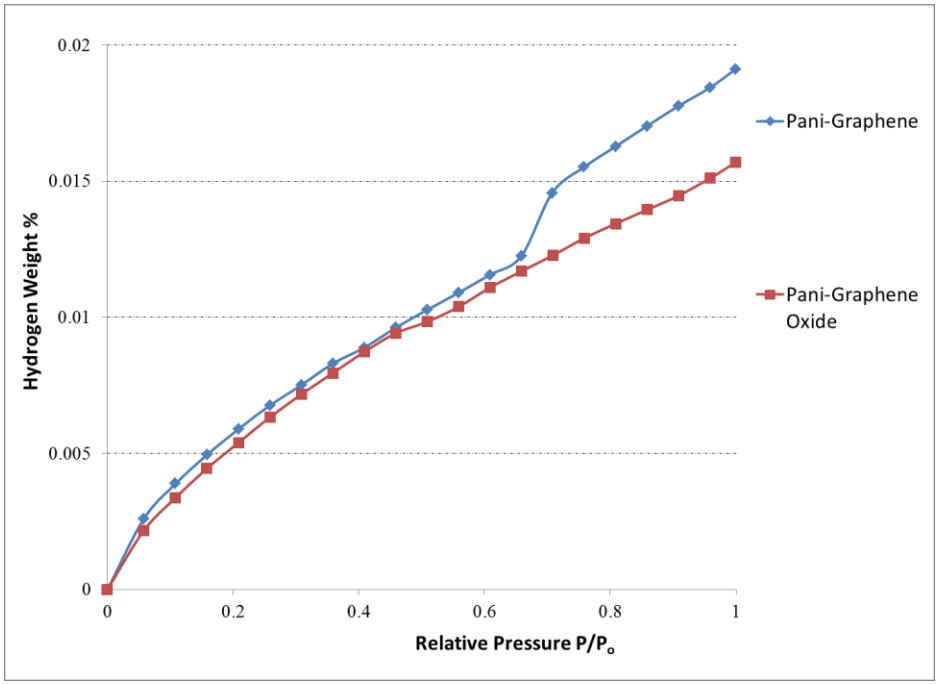

Figure 3.32 H_2 Sorption of Pani-G and Pani-GO at 77 K

3.7.6. Hydrogen Sorption at Room Temperature of Pani-Graphene

Hydrogen capacity was measured of the various ratios of Pani-graphene and also of Pani-GO complex in order to determine an optimum composite. Room temperature storage was of interest rather than liquid nitrogen temperature due to the low surface area of the Pani composites. Hydrogen storage was tested with PCT Pro 2000 with samples in the precision of 500 milligrams. Pressure-composition tests (PCT) showed which material has the greatest hydrogen storage capacity and at what pressure does it reach saturation. Figure 3.33 shows the PCT curves of Pani-graphene at the molar ratios of 1:1, 1:0.1, and 1:0.05. The saturation pressure for the 1:0.05 molar ratio sample was at 85 bar, yet was at 105 bar for the other samples. Saturation occurs when the composite has no more surface area and pore volume to store hydrogen. The highest capacity sample was the 1:0.1 ratio which reached a hydrogen storage of 0.58 weight %. The 1:1 molar ratio sample reached a hydrogen storage of 0.51 weight %.

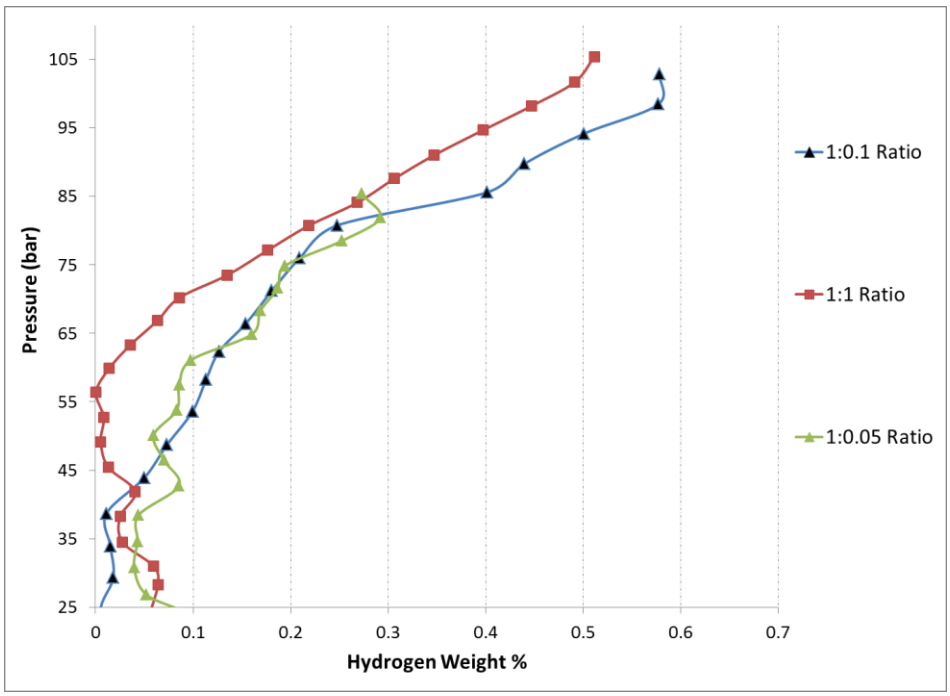

Figure 3.33 PCT of Pani-Graphene at Various Molar Ratios

3.7.7. Summary of Pani-G and Pani-GO Results

Polyaniline is a novel material that has unique optical and electronic properties. The synthesis route for Pani is a facile and cost-effective one. The method of synthesizing Pani was dilute oxidative polymerization with rapid mixing. Graphene and graphene oxide were incorporated into the Pani matrix in order to increase the hydrogen storage of the composite. FT-IR characterization proved that G/GO was successfully embedded in the polymer matrix while aniline was still sufficiently polymerized by APS. Surface area measurements proved that graphene at low molar ratios (1:0.05) does not block any of the pores and inherit surface area of Pani. The ratio of 1:0.05 was used for both graphene and graphene oxide polymeric composites. Liquid nitrogen temperature hydrogen capacity was at 0.016 wt. % and 0.019 wt. % for Pani-GO and Pani-G,

respectively. Hydrogen storage at room temperature showed that the sample of Pani-graphene with a 1:0.1 molar ratio stores the highest of hydrogen at 0.58 weight % at a pressure of 105 bars. This is still well short of the DOE targets for year 2015, yet it is an improvement from 0.1 weight %, which is the storage of Pani at room temperature.

3.8. Pani-GO Cross-Linked Composite

The highest surface area material of the cross-linked graphene oxide samples was the GO cross-linked with the solvent ethanol. The achieved surface area was 324 m^2/g from the GO control of 18.8 m^2/g. The storage capacity at 77 K was a relatively high value of 0.33 wt. %.

3.8.1. Method of Synthesis of Pani-GO (C.L.)

Two methods of synthesis were utilized and compared. The first being the GO is cross-linked using the solvothermal synthesis, with ethanol as the solvent, then incorporated into the Polyaniline substrate using the same method outlined in section 3.7.1, which will be called the "post-synthesis." The other method was to incorporate untreated GO into Pani using the synthesis in 3.7.1 then to cross-link the Pani-GO complex using the solvothermal process. This will be called the "pre-synthesis." The molar ratio of aniline to graphene oxide cross-linked was 1:0.05.

3.8.2. FT-IR Characterization Results

FT-IR was used to determine the extent of embedding the graphene oxide into the Pani matrix. It was also used to ensure aniline was still polymerized through the process

and no un-desired reactions occurred. Figure 3.34 shows the FT-IR spectrum of both synthesis methods of Pani-GO cross-linked along with the control sample of Pani-GO, which contains an un-treated form of graphene oxide.

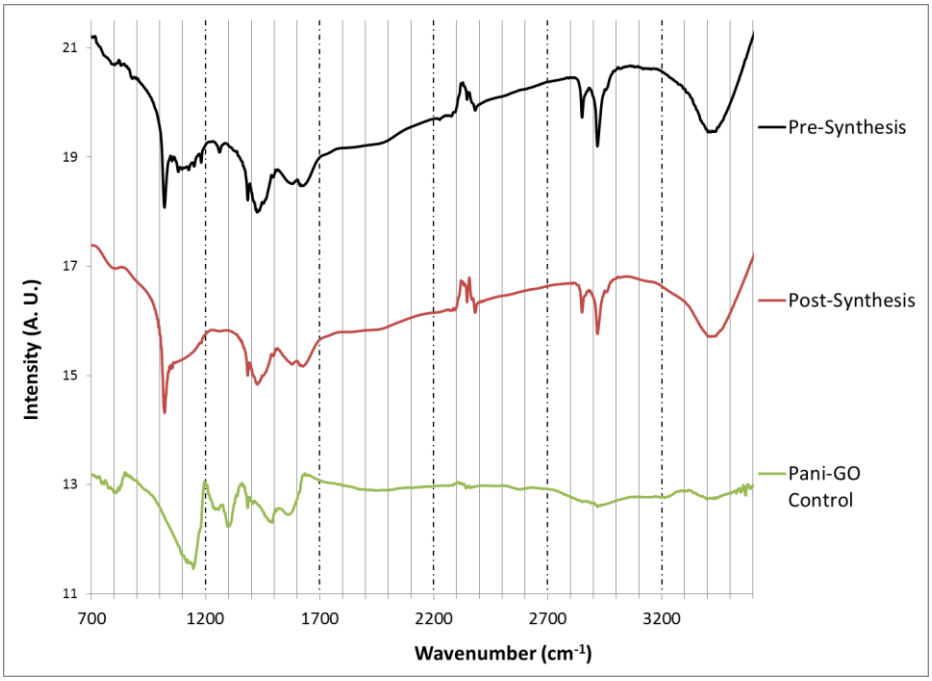

Figure 3.34 FT-IR SPectra of Pani-GO (C.L.) "Pre" and "Post"

The spectrum shows that the pre-synthesis and post-synthesis composites possess identical FT-IR spectra. Signals at 1300, 1450, and 1560 cm^{-1} represent signals from functional groups of Polyaniline. The peak at 1000 cm^{-1} shows the carbonyl group which proves the graphene oxide complex is present in the Polyaniline matrix.

3.8.3. BET Surface Area Measurements

BET theory was utilized with N_2 adsorption isotherms in order to determine the surface area of the Polyaniline-graphene oxide cross-linked composites. Table 3.9 shows and compares the surface area of these composites along with untreated Polyaniline and

Pani-GO composites. The pre-synthesis sample had a critical reduction in surface area to 1.1 m^2/g. The post-synthesis method reached a surface area of 36.6 m^2/g.

Table 3.9 BET Surface Area of Pre-Synthesis and Post-Synthesis

Sample Name	BET SSA (m^2/g)
Polyaniline	24
Pani-GO	31.1
GO C.L.	324
Pani-GO C.L.	36.6

3.8.4. H_2 Sorption at 77 K of Pani-GO C.L.

Hydrogen storage capacity was measured using Autosorb1 at liquid nitrogen temperature. Figure 3.35 shows the adsorption isotherms of the two methods of synthesizing Pani-GO cross-linked along with Pani-GO untreated as a control sample. Figure 3.35 shows the storage capacity for the post-synthesis and pre-synthesis Pani-GO cross-linked samples were 0.034 wt. % and 0.005 wt. %. The untreated complex has a storage capacity of 0.015 wt. %. The storage capacity was doubled by cross-linking the graphene oxide before adding to the Polyaniline complex.

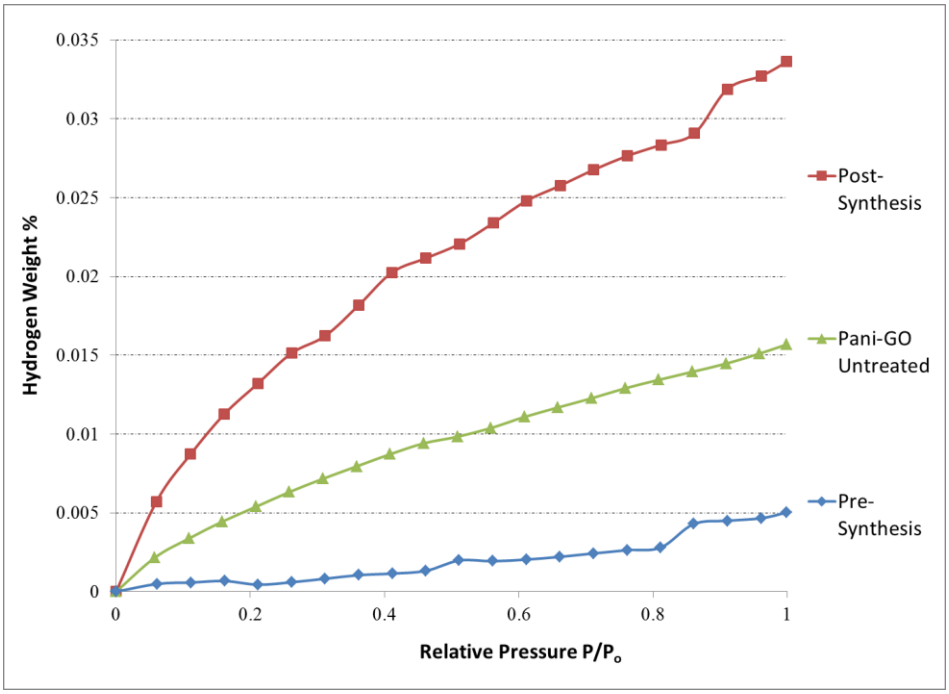

Figure 3.35 H_2 Adsorption of Pre- and Post-Synthesis Pani-GO C.L.

3.8.5. Summary of Pani-GO C.L. Results

The goal was to incorporate a higher surface area graphene oxide framework into the Polyaniline matrix in hopes of increasing the hydrogen storage capacity. FT-IR verified sufficient impregnation of graphene oxide into the polymeric matrix. BET theory determined that the "post-synthesis" method yielded a product with sustained surface area. Hydrogen sorption measurements proved that the product of Pani-GO cross-linked with ethanol increased the hydrogen storage from 0.015 wt. % to 0.034 wt. %, which is a dramatic improvement. However, this is a dramatic reduction compared to the capacity of graphene oxide cross-linked (without Pani), which is a storage of 0.33 wt. %. This decrease is due to the major reduction in surface area caused when adding the graphene oxide framework to the polymeric matrix.

3.9. Literature Comparison

To gain a better understanding of our research results it is important to compare them with previously published results of similar materials. Materials like graphene and polyaniline have already been well-established in literature with data on their hydrogen storage properties. Tables 3.10 and 3.11 compare the hydrogen storage values of graphene and polymeric materials, respectively, compared to literature values.

Table 3.10 Hydrogen Storage (77 K) of Graphene materials

Sample Name	H_2 wt. %
Graphene (lit.)	0.6 [10]
rGO	0.02
rGO-Pt	0.03
rGO-Ca	0.01

Table 3.11 Hydrogen Storage (77 K) of Polymeric Materials

Sample Name	H_2 wt. %
Pani (lit.)	0.10 [15]
Pani	0.05
Pani-G	0.019
Pani-GO	0.016
Pani-GO C.L.	0.034

Table 3.10 shows the literature value of hydrogen storage of graphene is 0.6 weight %. Differences between storage capacities of graphene from Dr. Dillon's research group and the reduced graphene oxide synthesized in our laboratory are probably due to surface area discrepancies [10]. Literature graphene has a surface area of 360 m^2/g compared to the graphene synthesized in our lab having only an area on the order of 10 m^2/g; this occurred due to difficulties of agglomeration when synthesizing graphene [10]. The platinum and calcium doped samples had a storage capacity of 0.03 and 0.01, respectively. This reduction in hydrogen storage at 77 K is probably due to the reduction in surface area occurring after doping the graphene samples. Surface area and pore volume are the major factors of hydrogen storage capacity at 77 K. Table 3.11compares polyaniline in literature from Dr. Germain's research group to polyaniline-graphene or graphene oxide composites [15]. The reduction from literature values for the hydrogen storage capacity most likely occurs because of the decrease in surface area when adding the graphene and graphene oxide materials to the polymer substrate. Our research suggests that adding graphene and graphene oxide materials to the polyaniline substrate, the hydrogen storage capacity values are less than values found in literature for pure polyaniline.

Chapter 4. Conclusion and Recommendation for Future Work

4.1. Overview

The objective of this thesis was to synthesize high surface area graphene-based complexes doped with metals in order to optimize hydrogen storage. Three aspects of hydrogen storage were dealt with in this thesis. Physisorption was optimized by attempting to increase the surface area of the graphene and graphene oxide complexes. Chemisorption was introduced when doping the materials with platinum nanoparticles, which chemically bond and disassociate hydrogen molecules for easier adsorption into the pores of the material. The adsorption enthalpy was also adjusted by introducing calcium doping to increase the attraction of the surface of the adsorbent to the hydrogen molecules of the adsorbate. Investigation and optimization of these three methods was pursued in order to determine an optimal storage material for hydrogen adsorption.

4.2. Physisorption

Physisorption optimization primarily consisted of increasing the accessible surface area and pores of the material for efficient hydrogen adsorption. Methods investigated to perform this task were exfoliation of graphene/graphene oxide and cross-linking of graphene oxide using diboronic acid spacers. Exfoliation of graphene oxide via platinum particles caused an increase of the surface area from 18.8 m^2/g to 65.2 m^2/g

using a 1 weight % ratio of platinum precursor. Graphene was not exfoliated by the platinum particles and remained an agglomerated surface area of 11 m^2/g. However, this exfoliation of graphene oxide did not cause an increase in hydrogen storage. The storage capacity at 77 K decreased in comparison with the untreated sample of graphene oxide. Thus it can be stated that the chemisorption component of platinum nanoparticles did not have a measurable effect on the hydrogen capacity of the samples.

Cross-linking of graphene oxide using diboronic acid spacers with various solvents via a solvothermal reaction was investigated. It was determined that ethanol was the most optimal solvent for the highest increase in surface area, which was 18.8 m^2/g to 324.2 m^2/g. This directly resulted in an increase of hydrogen storage at 77 K from 0.18 wt. % to 0.33 wt. %. This is the highest hydrogen storage material that was developed in this research. It is also the material with the highest surface area of 324 m^2/g.

4.3. Adsorption Enthalpy

Calcium doping was performed on the grapheme and grapheme oxide materials for the purpose of increasing the adsorption enthalpy. The adsorption enthalpy measures the attraction between the hydrogen molecules and the surface of the adsorbent. The desired range for the adsorption enthalpy is 15 – 20 kJ/mol. Calcium doping of grapheme resulted in very inconsistent results with enthalpies in the negative realm. This is due to its extremely low storage capacity at 77 and 87 K. Calcium doped grapheme oxide reached higher enthalpies at a maximum of 6 kJ/mol. This is more promising than grapheme, although still not in the desired range (15 – 20 kJ/mol) for room temperature storage.

4.4. Polymeric Complexes

Various samples of grapheme and grapheme oxide were embedded into a polyaniline matrix in hopes of increasing the adsorption capacities of the materials. It seemed that polyaniline was reducing the surface area and accessible pores of the grapheme/grapheme oxide complexes which caused a reduction of the hydrogen storage capacity. The most optimum storage material was obtained when the cross-linked grapheme oxide framework was synthesized with polyaniline to form a composite material. This material reached a capacity of 0.033 weight %, which is an increase from pure polyaniline, yet still distant from DOE targets for the year 2015. Room temperature storage of Pani-graphene was found to saturate at 0.6 weight %. This is also an improvement from Pani (untreated), yet still distant from the DOE targets.

4.5. Future Work

The most promising and direct method to reach hydrogen storage at room temperature is to investigate the adsorption enthalpy of a material. The adsorption enthalpy dictates at what temperature the material will most adsorb hydrogen. The ideal range for adsorption at 298 K of hydrogen is 15 – 20 kJ/mol. Computational works state that calcium atoms have the ability to increase the adsorption enthalpy to this range. The complexes doped with calcium in this thesis only had an increase to 6 kJ/mol, due to insufficient covering of calcium atoms or aggregation of the calcium atoms on the surface of the material. Finding a method to sufficiently dope the calcium atoms across the surface of a carbon-based material will lead to a higher adsorption enthalpy of hydrogen interaction. Literature reports computational studies on utilizing boron as anchoring

points for calcium doping. Problems arise in determining a synthesis route for the placement of the boron atoms in the specific anchoring points on the surface of the complex.

References

1. Houghton, J.T., *Climate change 2001 : the scientific basis ; contribution of Working Group I to the third assessment report of the Intergovernmental Panel on Climate Change*. 2001, Cambridge: Cambridge Univ. Press.

2. Crowley, T.J., *Causes of Climate Change Over the Past 1000 Years.* Science, 2000. **289**(5477): p. 270-277.

3. Vitousek, P.M., *Beyond Global Warming: Ecology and Global Change.* Ecology, 1994. **75**(7): p. 1861-1876.

4. Hillman, T. and A. Ramaswami, *Greenhouse Gas Emission Footprints and Energy Use Benchmarks for Eight U.S. Cities.* Environmental Science & Technology, 2010. **44**(6): p. 1902-1910.

5. R.W, B., *Global oil & gas depletion: an overview.* Energy Policy, 2002. **30**(3): p. 189-205.

6. Andreas, Z., *Materials for hydrogen storage.* Materials Today, 2003. **6**(9): p. 24-33.

7. Satyapal, S., et al., *The U.S. Department of Energy's National Hydrogen Storage Project: Progress towards meeting hydrogen-powered vehicle requirements.* Catalysis Today, 2007. **120**(3–4): p. 246-256.

8. Rzepka, M., P. Lamp, and M.A. de la Casa-Lillo, *Physisorption of Hydrogen on Microporous Carbon and Carbon Nanotubes.* The Journal of Physical Chemistry B, 1998. **102**(52): p. 10894-10898.

9. Nijkamp, M.G., et al., *Hydrogen storage using physisorption – materials demands.* Applied Physics A: Materials Science & Processing, 2001. **72**(5): p. 619-623.

10. Dillon, A.C. and M.J. Heben, *Hydrogen storage using carbon adsorbents: past, present and future.* Applied Physics A: Materials Science & Processing, 2001. **72**(2): p. 133-142.

11. Sakintuna, B., F. Lamari-Darkrim, and M. Hirscher, *Metal hydride materials for solid hydrogen storage: A review.* International Journal of Hydrogen Energy, 2007. **32**(9): p. 1121-1140.

12. Nicolais, L. and G. Carotenuto. *Metal-polymer nanocomposites*. 2005; Available from: http://search.ebscohost.com/login.aspx?direct=true&scope=site&db=nlebk&db=nlabk&AN=124404.

13. Chalk, S.G. and J.F. Miller, *Key challenges and recent progress in batteries, fuel cells, and hydrogen storage for clean energy systems.* Journal of Power Sources, 2006. **159**(1): p. 73-80.

14. Zaluska, A., L. Zaluski, and J.O. Ström-Olsen, *Structure, catalysis and atomic reactions on the nano-scale: a systematic approach to metal hydrides for hydrogen storage.* Applied Physics A: Materials Science & Processing, 2001. **72**(2): p. 157-165.

15. Germain, J., J.M.J. Fréchet, and F. Svec, *Nanoporous Polymers for Hydrogen Storage.* Small, 2009. **5**(10): p. 1098-1111.

16. Germain, J., et al., *High Surface Area Nanoporous Polymers for Reversible Hydrogen Storage.* Chemistry of Materials, 2006. **18**(18): p. 4430-4435.

17. Germain, J., J.M.J. Frechet, and F. Svec, *Hypercrosslinked polyanilines with nanoporous structure and high surface area: potential adsorbents for hydrogen storage.* Journal of Materials Chemistry, 2007. **17**(47): p. 4989-4997.

18. *Labnet Hermle Z200A Compact Centrifuge with rotor* [cited 2012 January 15]; Available from: http://www.teletronics-photography.com/cgi-bin/mivavm?/Merchant2/merchant.mvc+Screen=PROD&Store_Code=TI&Product_Code=HZCC&Category_Code=Medical.

19. *PureLab Glove Box System.* [cited 2012 January 15]; Available from: http://www.gloveboxes.com/he/2gb-glovebox.php.

20. *Heated Ultrasonic Cleaner with Digital Timer (6000 mL)*. [cited 2012 January 15]; Available from: http://www.mtixtl.com/heatedultrasoniccleanerwithdigitaltimer6000ml-sh150-6l.aspx.

21. *QSonica Sonicator Q500*. [cited 2012 January 15]; Available from: http://sonicator.com/sonicatorQ500.aspx.

22. *Laboratory Synergy Fritsch Planetary Mill P5*. [cited 2012 January 20]; Available from: http://www.labplanet.com/laboratory-synergy-fritsch-planetary-mill-p5-115v-05-6000-00.html.

23. Smith, B.C., *Fundamentals of Fourier transform infrared spectroscopy*. 2009: Taylor and Francis.

24. Niemann, M.U., *Development and investigation of novel nanostructures and complex hydrides for hydrogen storage [electronic resource] / by Michael Ulrich Niemann*. 2009, [Tampa, Fla: University of South Florida.

25. Dorset, D.L., *X-ray Diffraction: A Practical Approach.* Microscopy and Microanalysis, 1998. **4**(05): p. 513-515.

26. Brandon, D. and W.D. Kaplan, *Scanning Electron Microscopy*, in *Microstructural Characterization of Materials*. 2008, John Wiley & Sons, Ltd. p. 261-281.

27. Shaw, D.J., *Introduction to colloid and surface chemistry / Duncan J. Shaw*. 3d ed. ed. 1980, London ; Boston: Butterworths.

28. Quantachrome. *Quantachrome Autosorb 1 Series: Surface Area and Pore Size Analysis* [cited 2012 February 2]; Available from: http://www.quantachrome.co.uk/en/Surface_Area_and_Pore_Size_Analyzer-Autosorb-1.asp.

29. Gómez-Serrano, V., C.M. González-García, and M.L. González-Martín, *Nitrogen adsorption isotherms on carbonaceous materials. Comparison of BET and Langmuir surface areas.* Powder Technology, 2001. **116**(1): p. 103-108.

30. Zhu, Y., et al., *Graphene and Graphene Oxide: Synthesis, Properties, and Applications.* Advanced Materials, 2010. **22**(35): p. 3906-3924.

31. Guo, H.-L., et al., *A Green Approach to the Synthesis of Graphene Nanosheets.* ACS Nano, 2009. **3**(9): p. 2653-2659.

32. Mikhail I, K., *Graphene: carbon in two dimensions.* Materials Today, 2007. **10**(1–2): p. 20-27.

33. Dimitrakakis, G.K., E. Tylianakis, and G.E. Froudakis, *Pillared Graphene: A New 3-D Network Nanostructure for Enhanced Hydrogen Storage.* Nano Letters, 2008. **8**(10): p. 3166-3170.

34. Burress, J.W., et al., *Graphene Oxide Framework Materials: Theoretical Predictions and Experimental Results.* Angewandte Chemie International Edition, 2010. **49**(47): p. 8902-8904.

35. Wu, Z.-S., et al., *Synthesis of Graphene Sheets with High Electrical Conductivity and Good Thermal Stability by Hydrogen Arc Discharge Exfoliation.* ACS Nano, 2009. **3**(2): p. 411-417.

36. Villar-Rodil, S., et al., *Preparation of graphene dispersions and graphene-polymer composites in organic media.* Journal of Materials Chemistry, 2009. **19**(22).

37. Zhang, J., et al., *Reduction of graphene oxide vial-ascorbic acid.* Chemical Communications, 2010. **46**(7).

38. Lee, H., et al., *Calcium-Decorated Graphene-Based Nanostructures for Hydrogen Storage.* Nano Letters, 2010. **10**(3): p. 793-798.

39. Si, Y. and E.T. Samulski, *Exfoliated Graphene Separated by Platinum Nanoparticles.* Chemistry of Materials, 2008. **20**(21): p. 6792-6797.

40. Wang, J., et al., *Assembly of Polyaniline Nanostructures.* Macromolecular Rapid Communications, 2007. **28**(1): p. 84-87.

41. Germain, J., J.M.J. Frechet, and F. Svec, *Hypercrosslinked polyanilines with nanoporous structure and high surface area: potential adsorbents for hydrogen storage.* Journal of Materials Chemistry, 2007. **17**(47).

42. Huang, J. and R.B. Kaner, *Nanofiber Formation in the Chemical Polymerization of Aniline: A Mechanistic Study*. Angewandte Chemie, 2004. **116**(43): p. 5941-5945.

Appendices

Appendix A: Permissions of Copyright

JOHN WILEY AND SONS LICENSE TERMS AND CONDITIONS

Feb 22, 2012

This is a License Agreement between Anthony J D'Angelo ("You") and John Wiley and Sons ("John Wiley and Sons") provided by Copyright Clearance Center ("CCC"). The license consists of your order details, the terms and conditions provided by John Wiley and Sons, and the payment terms and conditions.

All payments must be made in full to CCC. For payment instructions, please see information listed at the bottom of this form.

License Number	2854430270016
License date	Feb 22, 2012
Licensed content publisher	John Wiley and Sons
Licensed content publication	Angewandte Chemie International Edition
Licensed content title	Graphene Oxide Framework Materials: Theoretical Predictions and Experimental Results
Licensed content author	Jacob W. Burress,Srinivas Gadipelli,Jamie Ford,Jason M. Simmons,Wei Zhou,Taner Yildirim
Licensed content date	Nov 15, 2010
Start page	8902
End page	8904
Type of use	Dissertation/Thesis
Requestor type	University/Academic
Format	Electronic
Portion	Figure/table
Number of figures/tables	2
Number of extracts	
Original Wiley figure/table number(s)	Scheme 1, Figure 1
Will you be translating?	No
Order reference number	
Total	0.00 USD
Terms and Conditions	

TERMS AND CONDITIONS

This copyrighted material is owned by or exclusively licensed to John Wiley & Sons, Inc. or one of its group companies (each a "Wiley Company") or a society for whom a Wiley Company has

Appendix A (Continued)

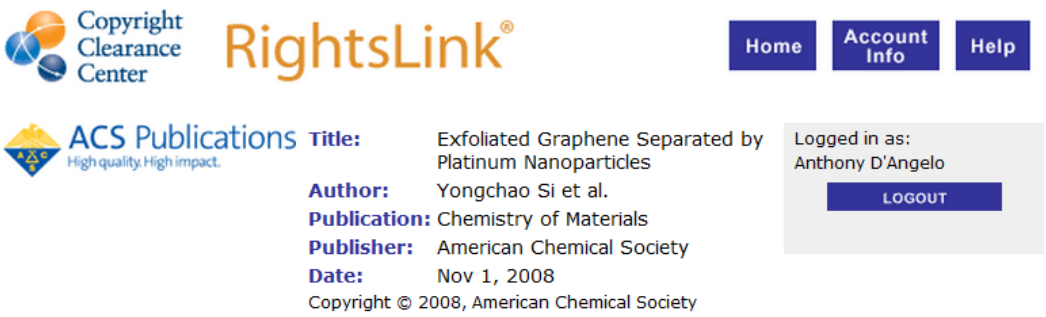

PERMISSION/LICENSE IS GRANTED FOR YOUR ORDER AT NO CHARGE

This type of permission/license, instead of the standard Terms & Conditions, is sent to you because no fee is being charged for your order. Please note the following:

- Permission is granted for your request in both print and electronic formats.
- If figures and/or tables were requested, they may be adapted or used in part.
- Please print this page for your records and send a copy of it to your publisher/graduate school.
- Appropriate credit for the requested material should be given as follows: "Reprinted (adapted) with permission from (COMPLETE REFERENCE CITATION). Copyright (YEAR) American Chemical Society." Insert appropriate information in place of the capitalized words.
- One-time permission is granted only for the use specified in your request. No additional uses are granted (such as derivative works or other editions). For any other uses, please submit a new request.

About the Author

Anthony Joseph D'Angelo was born in Virginia Beach, Virginia and lived in his hometown until he was 13. He moved to Melbourne, Florida and attended Rockledge High School. He attended undergraduate school at the University of South Florida – Tampa, where he would receive his Bachelors and Masters of Science degrees in Chemical Engineering. He researched hydrogen storage materials under Dr. Goswami with the Clean Energy Research Center. Anthony D'Angelo graduated in the spring of 2012 from USF and hopes to attend Boston University to pursue his doctorate degree in Materials Science and Engineering. He plans to pursue a career in academia with interests in renewable energy and inorganic chemistry. He desires to one day become a professor and start a company with a mission of alternative energy development.